2017

Rigorous Design of a Compact, Low-Speed, Open-Loop Wind Tunnel

Kharuna Ramrukheea
University of Windsor

Rigorous Design of a Compact, Low-Speed, Open-Loop Wind Tunnel

by

Kharuna Ramrukheea

A Thesis
Submitted to the Faculty of Graduate Studies
through the Department of Mechanical, Automotive & Materials Engineering
in Partial Fulfillment of the Requirements for
the Degree of Master of Applied Science at the
University of Windsor

Windsor, Ontario, Canada

2017

Rigorous Design of a Compact, Low-Speed, Open-Loop Wind Tunnel

by

Kharuna Ramrukheea

APPROVED BY:

D. Green
Department of Mechanical, Automotive & Materials Engineering

G. Rankin
Department of Mechanical, Automotive & Materials Engineering

J. Defoe, Advisor
Department of Mechanical, Automotive & Materials Engineering

May 26, 2017

Declaration of Previous Publication

This thesis includes one original paper that has been accepted for publication in conference proceedings, as follows:

Thesis Chapter	Publication title/ full citation	Publication status
Chapter 2, 3, 4, and 6	A First Principles-Based and Numerical Design Approach for Fluid Flow Systems with Application to an Open-Loop Wind Tunnel. Ramrukheea, K., Defoe, J. Proceedings of the 25^{th}Annual Conference of the Computational Fluid Dynamics Society of Canada, Windsor, ON, Canada, June 18-20, 2017.	Accepted

I certify that I have retained copyright to the above material in my thesis. I certify that the above material describes work completed during my registration as a graduate student at the University of Windsor.

I declare that, to the best of my knowledge, my thesis does not infringe upon anyone's copyright nor violate any proprietary rights and that any ideas, techniques, quotations, or any other material from the work of other people included in my thesis, published or otherwise, are fully acknowledged in accordance with the standard referencing practices. Furthermore, to the extent that I have included copyrighted material that surpasses the bounds of fair dealing within the meaning of the Canada Copyright Act, I certify that I have obtained a written permission from the copyright owner to include such material(s) in my thesis.

I declare that this is a true copy of my thesis, including any final revisions, as approved by my thesis committee and the Graduate Studies office, and that this thesis has not been submitted for a higher degree to any other University or Institution.

Abstract

Currently available literature regarding the design of fluid flow systems tend to focus on the specific system without providing a general guideline for how to address the design problem. This thesis focuses on developing such a general approach which is applied to the design of a wind tunnel meant for the University of Windsor. It is shown that, by applying the first principles of fluid mechanics to the problem, the components required, for operation of the wind tunnel within set constraints and requirements are identified. Numerical simulations are performed in two parts: 1) two-dimensional computational fluid dynamics simulations, which enable a parametric study of each component, and 2) three-dimensional computations, which provide a more accurate estimation of the performance of the wind tunnel. By following these steps, it is found that computational cost is greatly reduced by first sizing the components during the parametric study. The metrics used to assess the wind tunnel performance are the flow non-uniformity and the total pressure loss coefficient throughout the tunnel. The first principles based approach yields a set of components, respecting the constraints set while two-dimensional computations allows the determination of the wind tunnel dimensions and estimation of its performance, which is verified by a three-dimensional computation.

Employing this approach, a successful wind tunnel design rated with a maximum volume flow rate of 12.9 m^3/s at a test section inlet velocity of 40 m/s with the ability to be attached to different test sections is achieved. This wind tunnel comprises a fan followed by a constant area duct leading to a diffuser, which is attached to a flow conditioner. The last component is a nozzle directing the flow into the test section. The wind tunnel operates with an estimated 8% flow non-uniformity at the nozzle exit together with a total pressure loss coefficient of 0.238 based on the test section inlet dynamic pressure.

Acknowledgements

Words cannot express my gratitude towards my supervisor, Dr. Jeff Defoe, who has shown unlimited patience and encouragement throughout this project. Under his supervision, I have been able to acquire and enhance my knowledge in the field of computational fluid dynamics (CFD), all while adopting a more efficient thinking process in solving problems. I am very grateful for his training that has helped me develop skills at both a personal and a professional level.

Undoubtedly, this project would not be possible without the help of many, such as Mr. Andrew Jenner, who constantly assisted and provided advice from the beginning to the end of this project. I would like to also extend my thanks to Mrs. Angela Haskell who has provided support on several occasions.

A special thank you goes to all my colleagues in the Computational Fluid Dynamics Laboratory who have helped me understand and face the many difficulties in the CFD field. I want to thank Mr. Kohei Fukuda, Mr. Ravinder Gill, Mr. David Hill, and Mr. Krishna Patel for their continuous feedback. I am indebted to Dr. Gary Rankin, Mr. Sichang Xu, and Mr. Chris Peirone who were kind enough to allow me to use their computer resources.

Last but not least, I am forever grateful to my family and friends, without whose support accomplishing this graduate degree would be impossible. This work would not have been possible without the support of each and every one of you. I would like to express my gratitude to my mentor, Dr. Nihar Biswas, for his advice and support.

This work was funded by the University of Windsor. It involved the use of computational resources offered by the Shared Hierarchical Academic Research Computing Network (SHARCNET).

Contents

List of Figures

List of Tables

Nomenclature

Symbols

A cross-sectional area

C recovery coefficient

D duct diameter

L length

U axial velocity

W width

dA differential cross-sectional area

l fan outlet length

p static pressure

$RMS\%$ normalized root-mean-squared variation in velocity

s screen solidity

u velocity magnitude

w fan outlet width

dp differential pressure

du differential velocity magnitude

dx differential duct axial length

y^+ dimensionless wall distance

κ screen pressure drop coefficient

ρ density

ω total pressure loss coefficient

θ half diffusion angle

Subscripts

d diffuser

f fan

h honeycomb

i component inlet

n nozzle

o component outlet

$s1$ first screen

$s2$ second screen

t total quantity

ts test section

Superscripts

X mixed-out quantity

A area-weighted quantity

Abbreviations

MAME Mechanical, Automotive & Materials Engineering

RMS Root-Mean Square

CFD Computational Fluid Dynamics

CTA Constant Temperature Anemometry

PIV Particle Image Velocimetry

LDV Laser Doppler Velocimetry

RANS Reynolds-Averaged Navier Stokes

SIMPLE Semi-Implicit Method for Pressure-Linked Equations

Chapter 1

Introduction

To support teaching and research work within the Aerospace Option at the University of Windsor's Mechanical, Automotive & Materials Engineering (MAME) Department, a new wind tunnel is required. Currently, the department houses two wind tunnels which cannot accommodate the types of test sections required for the targeted area of study, which is turbomachinery. This thesis focuses on carrying out the design work for the wind tunnel by developing and employing an approach based on the application of the first principles of fluid mechanics. The design of specific test sections is not part of the scope of this work. With limited space allocation for laboratory equipment, the challenge of this project lies in designing a compact wind tunnel which can produce maximum volume flow rate of 12.9 m^3/s with a uniform flow of 40 m/s. With a Mach number of 0.118 at the test section inlet (the region of highest average velocity across the entire wind tunnel) the flow can be considered incompressible.

1.1 Objectives

The main goal of this research thesis is to design a compact wind tunnel and to develop a set of design guidelines for general internal fluid flow systems. These guidelines are generated according to insight gained through the application of an approach based on

the analysis from first principles of fluid mechanics applied to the problem of designing a wind tunnel with turbomachinery cascade and other test sections. The aim of this approach is to simultaneously achieve (1) a low total pressure drop, which sets the power required to drive flow through the tunnel, for a given flow rate and (2) a high level of flow uniformity at the test section inlet/ wind tunnel outlet. The large variety of types of test sections envisioned for use with this tunnel renders it impractical for the thesis scope to include test section design. Therefore, the uniformity at the tunnel outlet/test section inlet is the key figure of merit for the flow.

1.2 Introduction to the Wind Tunnel

This wind tunnel will provide flow for turbomachinery cascade test sections, among others. Thus, considered as a mass flow generator, this facility must provide high quality flow to the test section inlet, with the flexibility to accommodate different types of test sections. This section presents the constraints and requirements set for this wind tunnel design. An introduction to the different types of test sections allow the identification of required features of the tunnel.

1.2.1 Requirements

The wind tunnel must provide a maximum volume flow rate of 12.9 m^3/s at a test section inlet velocity ($\bar{U}^X_{ts,i}$) of 40 m/s; the minimum test section inlet velocity is about $0.5\bar{U}^X_{ts,i}$ m/s. The maximum performance is set based on expected Reynolds number and Mach number for the envisioned test sections. The maximum volume flow rate and corresponding maximum velocity sets the outlet area of the wind tunnel to be $A_{n,o} = 0.326m^2$. This combination of length and velocity scales yields test section Reynolds numbers on the order of 2×10^5, sufficient to ensure rapid turbulence transition, without Mach numbers entering the compressible flow regime.

The flow non-uniformity present at the nozzle outlet is evaluated by an area-weighted normalized root-mean square (RMS) variation in velocity, $RMS\%$. The full definition of this parameter is given in section 2.3.6; based on the literature, it should not exceed 10% at the nozzle outlet.

The tunnel needs to accommodate different types of test sections, including both internal and external flows. The types of test sections already envisioned include: 1) turbomachinery blade cascades, 2) semi-free jets, and 3) free jets. A brief discussion of the characteristics of each of these types of test sections follows.

Blade cascades are a long-standing tool for assessment of turbomachinery blade performance and in aerodynamics research[1]. A cascade consists of a stationary row of equally-spaced blades, which can be categorised as either linear or annular depending on the blade arrangements.

In a linear cascade, the blades are arranged in a straight line and the flow is turned by the blades as seen in Fig. 1-1. The turning angle may be large, possibly more than 90° for turbine blades.

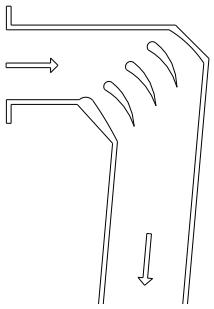

Figure 1-1: Linear cascade blade test section requiring large changes in flow direction.

In an annular cascade, the blades are arranged in an annulus, as seen in Fig. 1-2, so that blade turning imparts swirl to the flow.

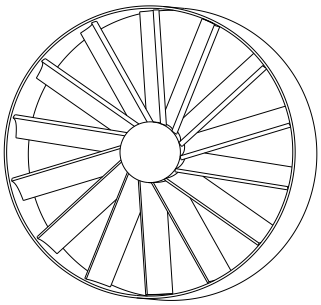

Figure 1-2: Schematic illustration of an annular cascade blade test section.

Enclosed test sections for assessing the performance of isolated airfoils can be limited in the amount of camber and/or the range of angles of attack available due to the presence of endwalls above and below the airfoil. The solution is to use a semi-free jet, as depicted in Fig. 1-3. The fluid can exit the test section at the top and bottom in addition to the usual test section outlet.

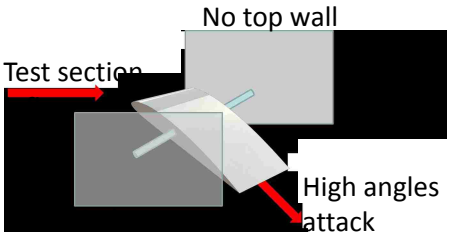

Figure 1-3: Semi-free jet test section.

Free jets can be used to measure aerodynamic forces on bodies smaller than the jet diameter. By means of a ground support, the body of interest is placed in the tunnel outflow jet, as illustrated in Fig. 1-4.

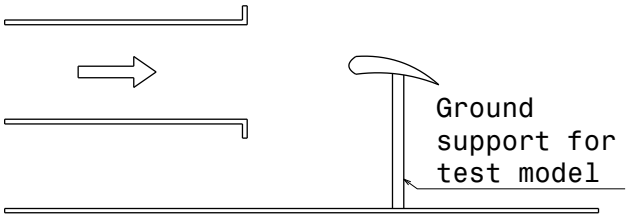

Figure 1-4: Free jet test section with ground platform to support test model.

The requirements of the tunnel can thus be summarized as follows:

1. There is a need to accommodate different types of test sections, including both internal and external flows.

2. Due to the variety in test sections, the wind tunnel will need to match circular test section inlet for annular cascades and free jets, and the rectangular cross-sections of linear cascades and semi-free jet test sections.

3. The difference in direction between the inflow and the outflow of a test section can be larger than 90°.

1.2.2 Constraints

The space occupied by the wind tunnel is limited by the room allocated, which is 13.4m long, 3.3m wide and 3.6m high. The total pressure drop through the passive components of the tunnel should be less than or equal to one fan outlet dynamic pressure. This limit is set based on the probable fan outlet velocity ($0.5\bar{U}^X_{ts,i}$), according to a survey of potential fans for this application, all while considering the estimated allowable total pressure drop that will be incurred when driving the the flow through the test section.

1.2.3 High Level Wind Tunnel Features to Address The Requirements and Constraints

Based on the requirements and constraints set, some of the features of the wind tunnel can be determined. First, an open-loop wind tunnel is selected to simultaneously address the issues of 1) limited space and 2) the requirement for the flow to undergo a turning of more than 90° in the test section. Unlike a closed-loop wind tunnel, an open-loop one can fit in a compact space, thus satisfying one of the requirements of

this project. Including a test section, in which flow would undergo a large amount of turning, would be challenging and costly for a closed-loop wind tunnel.

It is also less expensive to accommodate different test sections within an open-loop wind tunnel. To match the different test section inlet geometries, only the upstream component of the test section needs to be duplicated in the case of an open-loop wind tunnel. Within a closed loop wind tunnel, both the upstream and downstream components of the test section would need to be replicated to match the inlet and outlet of the test sections.

Within an open-loop wind tunnel, a pusher style fan or a suction configuration can be used to drive the flow. With the former option, the flow is driven into the test section, located downstream of the fan. In the suction style, air is drawn into the test section from the environment. A suction fan would require separate bellmouth inlets to draw air into the tunnel for each type of test section used.

To address the variety of possible test sections, some type of adaptation is required to accommodate both round and rectangular test section inlets. The largest allowable cross section of the wind tunnel is 2.0 m wide by 2.0 m high due to clearance requirements. The maximum length of the tunnel, including the fan, is restricted to 7.8 m to ensure adequate space is allocated for the test section.

1.3 Challenges

Current literature shows a lack of general guidelines for fluid flow system design that are not overly based on empiricism. Empirical studies are limited by the number of wind tunnels which are investigated. Further, due to the time-consuming experiments that need to be carried out, these studies focus on only one aspect of the wind tunnel design. Therefore, they can fail to capture interesting flow behaviour affecting the performance of the facility at different locations along the wind tunnel.

The compact nature of the wind tunnel requires a rigorous design process to simultaneously achieve high flow uniformity and low losses. Another challenge of this project is to establish a wind tunnel design with an overall geometry simple enough to manufacture.

1.4 Key Outcomes

The key outcomes of this thesis are:

1. A design approach which can be applied to other fluid flow systems is developed. This approach involves applying the first principles of fluid mechanics to the design problem to identify the different components required to satisfy the constraints and requirements set. This is followed by numerical computations which are performed in two stages. Two-dimensional computational fluid dynamics (CFD) computations are employed in a parametric study of each component to determine the best geometry with respect to the figures of merit. Three-dimensional CFD computations are carried out to provide a more accurate estimation of the performance of the complete, sized wind tunnel.

2. A fully operational open-loop subsonic wind tunnel addressing the requirements and constraints, has been installed within the MAME department at the University of Windsor. The wind tunnel is predicted to provide a flow with non-uniformity of 8.07% all while keeping the total pressure drop at 0.238 times the test section inlet dynamic pressure. Equipped with a pusher type fan, it can provide a maximum volume flow rate of 12.9 m^3/s at a test section inlet velocity of 40 m/s. It also comprises two nozzles, which can easily be mounted, to deal with the different test sections.

3. A commissioning plan is set up for testing the wind tunnel. This plan can be altered for use for other testing such as that of the different test sections.

1.5 Scope of Thesis

This thesis is organized such that Chapter 2 provides a review of relevant literature. The approach used to design this wind tunnel is described in Chapter 3 while the results are discussed in Chapter 4. Details about the wind tunnel assembly, coupled with other additional devices to enhance its performance are illustrated in Chapter 5. Conclusions and recommendations are established in Chapter 6.

Chapter 2

Literature Review

This chapter presents relevant past work in the field of fluid flow system design. The focus is on wind tunnels and common components of such equipment. The metrics used to evaluate the performance of the wind tunnel, as well as previous work done in assessing wind tunnel performance are also reviewed. The shortcomings of the presented studies are also identified.

2.1 Established Design Approaches for Specific Fluid Flow Systems

Several studies present design approaches for different specific fluid flow systems such as work done by Vivek et al. [2], where CFD is applied in the design of the main vessel cooling system for pool-type fast nuclear reactors. Detailed parametric studies regarding the turbulence models which can be used concluded that the $k - \varepsilon$ turbulence model can provide as accurate results as can the other turbulence models considered. Further numerical calculations led to the conclusion that the CFD model should make use of the second order upwind scheme. Before simulating the convection and conduction processes taking place in the cooling system, this CFD model

is validated by comparing the results obtained from the calculations, when applied to the main vessel cooling circuit of a Japanese reactor, to those obtained during experiments found in the open literature. Two-dimensional CFD successfully allowed the determination of the amount of sodium flow rate required to maintain a certain main vessel temperature, while three-dimensional CFD enabled the discovery of how the manufacturability of an oval structure affects the circumferential temperature difference in the main vessel. This study is successful in illustrating how a CFD based approach can be used to model and design a main vessel cooling system. Yet, by focusing only on the cooling system's features without providing a general guideline of how this approach can be applied to other systems, it is representative of that found in the literature in that the approach is applicable to only a narrow class of problems. This thesis is based on a general approach, which can be applied to other design problems.

Another example of a design approach being established for a specific class of fluid flow system is presented by Calautit et al. [3]. The authors provide a design approach of comparing CFD calculations against experimental data for a subsonic, closed-loop wind tunnel which comprises four corners with guide vanes, a contraction, a diffuser, a test section, and an axial fan. Using ANSYS Fluent, three-dimensional CFD computations of different guide vane configurations showed that the presence of guide vanes only upstream of the test section improved the flow uniformity by 36%, while having a combination of both upstream and downstream guide vanes led to a 65% improvement. Since it was clear that the flow conditions in the component upstream of the test section affected that in the test section, it was concluded that the design of the upstream vanes, leading to the test section, should be closely monitored. CFD calculations of the wind tunnel, with an empty test section, and the case of a block within the test section, were assessed by comparing the numerical results to those obtained from the experimental setup. Though this paper provides a very good

description of the design approach adopted for a wind tunnel, it is limited to closed-loop wind tunnels. The requirements for the current wind tunnel to accommodate test sections with a wide variety of turning angles necessitates an open-loop design and thus precludes the use of the authors' approach.

The work presented by Mehta [4] describes general design rules of several components for a blower type wind tunnel. These rules are based on a review of the layout and performance of wind tunnels developed up to that point. The work is focused on wide-angle diffusers, the use of screens within them, and centrifugal blowers. Section 2.3 discusses how these rules, which have been derived by the author, affect the design of each component. While this is a good resource to start with, the fact that this paper is based on different wind tunnels which were known to have performed "satisfactorily" up to that point (1979) implies that there could be more up-to-date studies about the matter. For example, limited computational resources available restricted researchers' ability to fully investigate the fluid flow within the wind tunnel. They could only assess the performance of a wind tunnel based on experiments, and were focused on one aspect of the wind tunnel at a time, due to the time-consuming aspect of experimental work. Therefore, this thesis aims at enhancing the literature by providing a design approach based on the analysis of first principles of fluid mechanics and CFD calculations.

2.2 Classification of Wind Tunnels

With the common aim of providing uniform flow within the test section, wind tunnel designs vary over a wide range due to different applications (aeronautical and automotive among others), and the continuous emergence of innovative designs for new tasks. At the highest level, wind tunnels can be divided into those which are open-loop or into those which are closed-loop. While the construction of an open-loop

tunnel is simpler than that of a closed-loop one, the latter reduces the power required to drive a given flow rate [5]. An open-loop configuration raises concerns with respect to noise treatment required to prevent any environmental problems [6]. Yet, since this setup provides more flexibility with regards to the varying test section geometry, the need for an open-loop wind tunnel is re-affirmed.

2.3 Complete Wind Tunnel Design

This section is divided in six parts with focus on the different common components of a wind tunnel, the use of CFD in designing a wind tunnel, and the metrics used throughout this thesis to assess the performance of the wind tunnel.

2.3.1 Fan

Cattafesta et al. [7] indicate that fans and compressors are the two primary drive systems for a wind tunnel. To drive air through a wind tunnel, a compressor can be used to provide pressurised air from a storage tank. Alternatively, a fan, which can be axial or centrifugal, drives air through the wind tunnel by pushing or pulling it through the test section. The main advantage fans hold over the compressors is the ability to continuously provide air to the test section. The latter can only provide a fixed amount of air, restricted by the storage tank's capacity, which limits the duration of an experiment.

Based on the review of several wind tunnels, Mehta [4] came to the conclusion that a centrifugal fan provides a steady and efficient operation over a wider range of flow coefficients compared to an axial fan. Rated by the volume flow rate and the static pressure rise required to drive fluid through the wind tunnel, a fan can be further categorized based on its blade shapes. According to Mehta, aerofoil type fans can run with reasonable steadiness and efficiency over a wide range of flow conditions,

thus making it an ideal candidate to run an open-loop wind tunnel.

Bradshaw [8] describes how the outflow from a centrifugal fan is far from uniform. This flow phenomenon is mainly due to the span of the rotor being only half of the width of the volute casing, a feature that the manufacturers used to match the "blower characteristics to a typical low-velocity ventilating system without using a long conical diffuser". By investigating the flow within a wind tunnel, which is meant to provide low-turbulence flow with or without a diffuser, the author found that with adequate use of screens and a flow conditioner, the non-uniformities can be eliminated. Yet, it is emphasized that non-uniform flow from the blower, notably the presence of thick boundary layers, can lead to separation and thus increase the losses and flow unsteadiness within a wide-angle diffuser. Available literature [7, 4, 8] indicates that a centrifugal fan is an excellent candidate for an open-loop wind tunnel. Since no accurate prediction of the outflow from the fan is available, this thesis provides measures that can be implemented to address the potential, harmful non-uniformities at the outlet of centrifugal fans.

2.3.2 Diffuser

It is a common requirement to have flow mixing within a wind tunnel. The associated power required to drive the fan is proportional to the cube of the flow speed at which mixing occurs. Therefore, to reduce the flow speed within a duct system, it is common to make use of a diffuser, a duct section in which fluid flows from a small cross-sectional area to a large one. As described by Mehta and Bradshaw [9], flow within a diffuser depends on its geometry, which is defined by the area ratio, the diffuser angle, the wall contour and the cross-sectional area. Barlow [6] adds that it is often desirable to reduce the flow speed within a short distance without the onset of flow separation, thus making diffusers critical components of a wind tunnel design. Regions of flow separation cause total pressure losses and usually result in severe flow

asymmetry and unsteadiness. Mehta [4] identifies that another feature that can lead to flow separation is the presence of sharp inlet corners; by filleting these corners, this problem can be avoided.

The effect of flow separation in diffusers has been extensively studied; Reneau et al. [10] describe the four regimes of fluid flow within which a two-dimensional diffuser (with expansion between only one pair of walls) can fall. These four regimes, separated and indicated by means of a diffuser stability map, are empirically based on "water table" studies in which dye injection is used to visualize the flow behaviour within diffusers [11, 12, 13, 14]. These regions were verified when similar experiments were performed with air as a fluid by Reneau et al. [10], Cochran et al. [12], Feil [13], and Johnston et al. [14]. This diffuser stability map identifies the geometrical constraints for which flow within a planar diffuser can reach better pressure recovery with slightly separated flow. The constraints of importance in this case are the diffusion angle, 2θ, and the diffuser axial length to inlet width ratio, $L_d/W_{d,i}$; the combination of these two parameters indicates the regime within which a diffuser, as illustrated in Fig. 2-1, will operate.

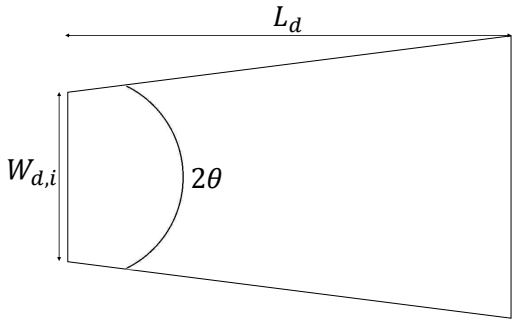

Figure 2-1: Geometric parameters describing a two-dimensional diffuser.

The "No Appreciable Stall" regime comprises diffusers with angles of diffusion of no more than 22. Within this area of the chart, it is still possible to observe small areas of stall (flow separation), depending on the thickness of the boundary layer.

Within the "Large Transitory Stall" regime, the region of separation continuously appears on either of the two diverging walls; while in the "Two-Dimensional Stall" regime, the separation occurs near the throat and follow only one diverging wall. The "Jet Flow" regime is one within which flow separation occurs along both diverging walls, originating from the throat area. While this study assists in designing a diffuser while avoiding the occurrence of separation, it presents a considerable limitation in that it is only applicable to planar diffusers. For the purpose of this thesis, the diffuser stability map is used to locate the regime within which the designed diffuser lies, thus limiting this wind tunnel design to the use of a planar diffusers.

Two types of diffusers commonly referred to are the exit diffuser and the wide angle diffuser [9, 4, 6]. As the name suggests, the exit diffuser is located downstream of the test section with a 'gentle' expansion of no more than 5°-10°. This diffuser is implemented to reduce the dynamic pressure of the jet, hence lowering the total pressure loss, that is released at the end of the tunnel. Yet, for ease of changing test sections, and to keep a wind tunnel as compact as possible, this component tends to be omitted.

While flow separation is undesirable, this effect cannot be avoided in wide angle diffusers, which are meant to connect the blower to the settling chamber, a duct allowing flow to mix. Barlow [6] describes a wide angle diffuser as one in which the rise in cross-sectional area is so drastic that boundary layer control mechanisms have to be employed to avoid the onset or the continuance of flow separation. Based on the review of wind tunnels known to perform satisfactorily, Mehta [4] provides a list of potential boundary layer control devices including a splitter system which can increase the total displacement thickness to reduce the diffusion angle; suction slots which are intrinsic to the diffuser wall, with regions of high velocity (upstream of the slot) and low velocity (downstream of the slot); trapped vortices which can force mixing with the core stream to energize the boundary layer; screens creating

regions of contraction and sudden expansion to mix out the flow; and vanes which can guide the inlet flow to improve diffuser performance. Compared to the listed options, Mehta and Bradshaw [9] established that the most common option used for economical reasons is the use of mesh screens.

As discussed by Greitzer [15], screens energize the boundary layer to delay the onset of flow separation. The presence of screens within a wind tunnel system leads to additional total pressure losses. The total pressure drop associated with a screen is determined using equation 2.1 given by Greitzer. This total pressure drop is related to its solidity ratio and velocity as follows:

$$\Delta p_t = \frac{1}{2}\kappa\rho u^2 \tag{2.1}$$

where ρ is the fluid density, u is the flow velocity magnitude, and κ is the screen pressure drop coefficient, which can be determined using equation 2.2, given by Cornell [16]. This equation indicates how κ depends only on the screen solidity ratio s.

$$\kappa = \frac{0.8s}{(1-s)^2} \tag{2.2}$$

Noui-Mehidi et al. [17] studied the fluid behaviour of an asymmetric diffuser to determine the impact of a combination of perforated plates within it. Based on the findings made by Sahin and Ward-Smith [18] about flow control being achieved with perforated plates close to the diffuser exit and an upstream location in the range of $0.150L_d$ to $0.290L_d$, Noui Mehidi et al. investigated seven combinations of four perforated plates with porosities of 45% within the diffuser. These screens were inserted through slots in the diffuser walls at $0.050L_d$, $0.250L_d$, $0.590L_d$ and $0.950L_d$. Using Laser Doppler Velocimetry and wall static pressure measurements, the flow properties were measured with the help of uniform rectangular mesh grids. The authors demonstrate that with four screens, the flow non-uniformity is at its lowest;

however, the pressure recovery is poor. It was also determined that two screens are sufficient to achieve flow uniformity; however, in the case of an asymmetric diffuser, an additional one is required. The findings of the study presented by Noui-Mehidi are used for the design of a wide angle diffuser with screens in this thesis.

2.3.3 Flow Conditioner

Cattafesta et al. [7] describe a flow conditioner as a duct section comprising a honeycomb, screens and a settling duct. When fluid flows through the honeycomb structure, the flow is aligned with the axis of the tunnel and the large scale flow unsteadiness is broken into smaller scales. Screens then further decay these turbulent fluctuations. To allow smaller scale flow unsteadiness to decay, a sufficiently long settling chamber is required while keeping the boundary layer growth to a minimum. Barlow et al. [6] indicate that compared to circular and square shaped cells, hexagonal cells are popular due to their low pressure drop coefficient. When compared to circular cells, the hexagonal cells are joined together at each of their vertex without creating any gaps. Also, according to Hales [19], a hexagonal grid leads to the least total perimeter when "a surface is divided into regions of equal area," thus leading to less total pressure drop due to skin friction.

Barlow et al. [6] also indicate that the best performance of a honeycomb can be achieved when its length to cell hydraulic diameter ratio is in the range of 6-8. While these rules have been used in the design of wind tunnels, the authors do not deny the fact that these have originated from observations of many arrangements. Further, this range is based on assumptions that may or may not be valid for a particular wind tunnel application. Therefore, the validity of such rules can be questioned for different wind tunnel design.

On a practical point of view, Barlow et al. [6] add that the honeycomb structure should be rigid enough to withstand the force imposed by the high speed flow. With

respect to screen implementation downstream of the honeycomb, screens or honeycombs of large cross-sectional area are difficult to make sufficiently rigid. To cover the large surface area, screens have to be spliced together, which is accomplished by brazing the widths of the screens together. The irregularities that result from the brazing have the potential of introducing turbulence. Therefore, based on this review, it can be seen that a honeycomb coupled with a settling chamber is required, while the need for screens depends on the cross-sectional area across which they will be fitted and the total pressure drop the screens will cause.

2.3.4 Nozzle

Several authors such as Cattafest et al. [7], Mehta and Bradshaw [4, 9], and Barlow et al. [6] agree that the nozzle is a critical wind tunnel component used to increase the mean velocity of the flow and to align the flow into the test section, thus determining the flow quality within the test section. As indicated by Morel [20], the acceleration achieved within the nozzle serves different purposes. For instance, due to the favourable pressure gradient within it, it is an aid to reduce the mean flow non-uniformities and to achieve a homogeneous flow at the test section inlet. Similarly, it scales down the turbulence level by breaking large scale eddies into small ones. In addition to achieving high flow uniformity and avoiding flow separation, minimum exit boundary layer thickness coupled with minimum contraction length are desirable attributes for a nozzle. The presence of wall curvature is required to avoid the risk of flow separation due to locally adverse pressure gradients near the walls; thus, a design satisfying these criteria would ensure that separation is just avoided and that the exit non-uniformity presents a velocity variation of $\pm\frac{1}{2}\%$ outside the boundary layer. This near-wall pressure gradient is governed by the flow curvature near the walls. To reduce this curvature, and hence to avoid flow separation, a nozzle's length should be maximized; however, since cost and thick exit boundary layers are of concern, this

makes it a less realistic design.

Based on the assessment of the "successful" wind tunnels, Mehta [4] states that the nozzle contraction ratio should be between 6 and 9. Mehta and Bradshaw [9] state that a smooth flow of air through the nozzle exit is important, due to its impact on potential flow separation. Therefore, the overall shape of the nozzle does not matter as much as does the geometry near the nozzle exit. It is emphasized that the nozzle's curved section should smoothly join the parallel sections such that the first and second derivatives of the curve at these meeting points are zero.

Nozzle design has been heavily influenced by the work done by Morel [20], in which the author developed charts for wind tunnel contractions using an inviscid, incompressible flow analysis. The numerical approach, enforced with the use of a computer program of the streamline curvature type (developed by General Motors Detroit Diesel-Allison Division), focuses on the investigation of one commonly used group of wall nozzles with the shapes being defined by two cubic arcs smoothly joined. For different wall shapes, the wall pressure coefficients at the inlet and outlet are calculated using equation 2.3, which is derived from the application of Bernouilli's equation given by equation 2.4.

$$C_p = 1 - \left(\frac{U_{n,o}}{U_{n,i}}\right)^2 \tag{2.3}$$

$$p + \frac{1}{2}\rho U^2 = constant \tag{2.4}$$

These coefficients are used to create the design charts from which the nozzle length and shape can be derived. While this study has served as a good basis for several nozzle designs, it is limited to one group of nozzles with contours of specific shapes. With current advances made in the CFD field, other groups of nozzle shapes could be investigated with special attention to different independent variables. This thesis

aims at making use of this tool to design the nozzle without the restriction on the number of independent variables that can be studied at a time.

2.3.5 Implementation of CFD to Capture Fluid Flow Behaviour

When compared to experimental investigations, CFD simulation of the flow within a wind tunnel provides an inexpensive, in terms of time and money, estimation of the fluid behaviour. To capture all flow behaviours within the wind tunnel accurately, the choice of turbulence model for the numerical calculations is critical, especially when flow separation is expected. An investigation carried out by Bardina et al. [21] showed that the Shear Stress Transport (SST) model by Menter [22] most accurately captures the details of separated flows. The authors compared and evaluated the performance of four popular turbulence models: the two equation k-ω model of Wilcox [23], Launder and Sharma's [24] two equation k-ϵ model, the two equation SST model, and the one equation Spalart-Allmaras model [25]. The evaluation was carried out by comparing against experimental data for ten turbulent flows. The application of these models to the case of a separated boundary layer, which was one of the turbulent flows investigated, led to the conclusion that the SST model is the best at capturing flow separation.

More recent work, such as that presented by Moonen et al., demonstrates how CFD is effective in predicting the flow behaviour within a wind tunnel [26]. The authors acknowledged the limited use of CFD in wind tunnel design; thus, the purpose of the study was to establish a methodology for numerically modelling the flow conditions in the full scale Jules Verne climatic closed-loop wind tunnel. Using a k-ϵ model, steady state three-dimensional CFD simulations were carried out to determine the total pressure loss and the flow rate within the test section. Unlike the conventional approach of modelling the flow just within the test section, the CFD simulation was carried out for the model of the entire wind tunnel to obtain more accurate results.

The simulations were performed for two cases, one with an empty test section and the other comprised a test model in the test section. By comparing the CFD results to available experimental results, this methodology of modelling the entire wind tunnel provides velocity values with an error of no more than 10%. The author concluded that the accuracy of the results from simulating the full model was 2-4 times better than the conventional CFD analysis of the test section only. This paper provides a basis for implementing the use of CFD as a tool in wind tunnel design and testing.

2.3.6 Metrics for Wind Tunnel Performance Assessment

A key parameter for assessing wind tunnels is the test section inflow uniformity. The metric used for this assessment of the wind tunnel performance is defined by Noui-Mehidi [17] as the normalized RMS variation in velocity defined in equation 2.5:

$$RMS\% = 100\sqrt{\left(\frac{U_{RMS}}{\bar{U}^A}\right)^2 - 1} \tag{2.5}$$

where

$$U_{RMS} = \sqrt{\frac{1}{A}\int_A U^2 dA}, \tag{2.6}$$

and

$$\bar{U}^A = \frac{1}{A}\int_A U dA. \tag{2.7}$$

U is the local flow velocity, $\bar{U}$ is the area-averaged value of the local velocities normal to a surface of cross-sectional area A. Area-averaging is employed since it is the profile of the velocity that is of concern. An $RMS\%$ value of 0 represents a perfectly uniform flow The other metric used to assess the performance of the wind tunnel is the total pressure loss coefficient between the inlet and outlet positions of a component, given

by

$$\omega_{io} = \frac{\bar{p}_{t,i}^{X} - \bar{p}_{t,o}^{X}}{\frac{1}{2}\rho(\bar{U}_{ts,i}^{X})^2} \tag{2.8}$$

where $\bar{p}_t^X$ is the mixed-out average total pressure across the cross-section at the component inlet i and outlet o. Mixed-out averaging at constant area is used to capture the additional eventual downstream loss rather than simply the local loss. This operation is defined in Greitzer et al. [15] for incompressible flow as

$$\bar{p}_t^X = \frac{1}{A}\int_A p dA + \frac{1}{A}\int_A \rho U^2 dA - \frac{1}{2}\rho\left(\bar{U}^X\right)^2 \tag{2.9}$$

These metrics are used to evaluate the tunnel's performance at different locations. The $RMS\%$ provides an indication of the flow non-uniformity while ω gives a non-dimensional indication of the total pressure drop; this is needed to know the required fan pressure rise.

2.4 Wind Tunnel Commissioning

To conclude the process of a wind tunnel design, commissioning of the system is required to ensure its operation is as per the requirements set. Commissioning of a wind tunnel can be referred to as performance analysis, facility characterization or flow quality determination. All these processes, with the same goal, can be applied to a newly built wind tunnel or to an existing one after undergoing any modifications or as part of a maintenance routine. Cattafesta et al. [7] discuss three common experiments carried out to ensure that the wind tunnel operates according to the set design criteria. These measure (1) flow uniformity, (2) turbulence characteristics, and (3) acoustics and vibrations. The actual experiments required for commissioning a wind tunnel would however depend on what the design criteria are.

Once these experiments are determined, the equipment required for these are established. For instance, to determine the flow uniformity, the velocity profile can be captured by measuring the values by traversing a Pitot static probe or a Pitot probe throughout the test section or more advanced equipment such as hot wires configured for constant temperature anemometry (CTA), particle image velocimetry (PIV), or laser doppler velocimetry (LDV) can be used.

Harvey [27] experimentally evaluated the performance of the Naval Postgraduate School Mechanical and Aerospace Engineering wind tunnel, which was re-installed and calibrated, to determine whether it was suitable for research and teaching purposes. With the use of pressure transducers attached to a Pitot static tube, wall static pressure taps, a pressure rake, and a hot wire anemometry system coupled with a rectangular traverse system, the author determined the wall static pressure distribution, total pressures across planes at different axial locations, the wall boundary layer characteristics, and the spectral energy distribution at selected points. With the help of a data acquisition processor with analog to digital conversion coupled with an in-house developed LabVIEW software, the author was able to determine that the new maximum axial speed was only 84% of the tunnel's rated speed. The flow uniformity was determined to be within$\pm$7% of the mean freestream velocity with the use of the pressure rake; the turbulence intensity was obtained within the range of 3%. An approach similar to the one described by Harvey is adopted for the planned commissioning of this wind tunnel.

2.5 Aspects of the Literature Used in this Study

In this work, the uniformity metric from the work of Noui-Mehidi et al. [17] is used for assessing flow non-uniformity from simulation data. The loss coefficient is determined by making use of the mixed out average given by Greitzer et al. [15]. Since available

literature provide guidelines that are constrained to specific fluid flow system, or simply empirical, a new approach is developed based on a component-by-component level assessment. While designing the wind tunnel, the rules established by Mehta [4], Mehta and Bradshaw [9], and Barlow [6] are taken into consideration. The diffuser stability map is used for the initial design of the component, and initial locations of screens (if any) are based on the results found by Noui-Mehidi.

Chapter 3

Approach

The design approach adopted for the wind tunnel is illustrated in Fig. 3-1. One-dimensional control volume analysis is employed to identify the required components. Based on the resulting components, a parametric study, using two-dimensional CFD computations, is performed to obtain final dimensions of the components. Three-dimensional CFD calculations provide an enhanced estimation of the complete wind tunnel performance. A Computer Aided Design (CAD) model of the entire tunnel is then created to enable fabrication.

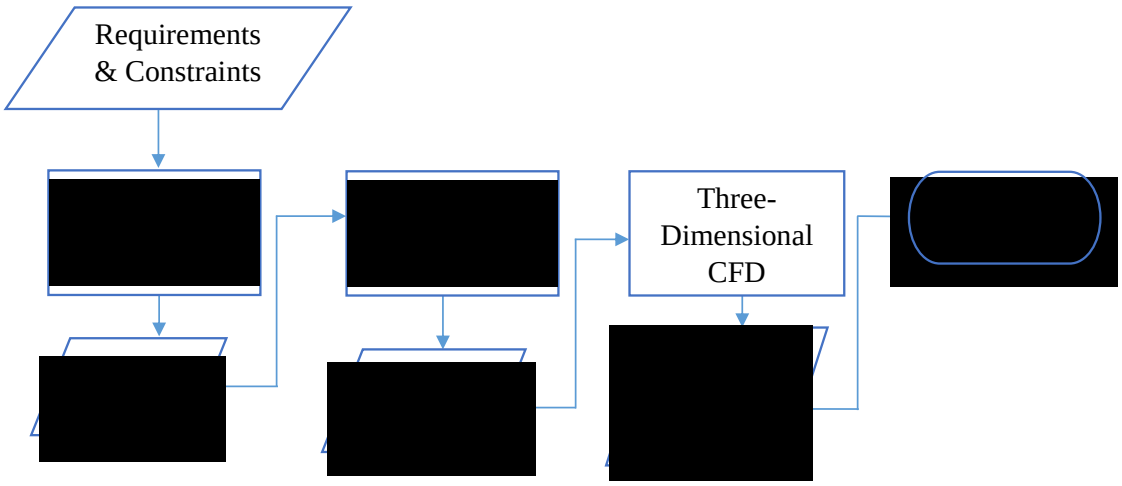

Figure 3-1: Flowchart illustrating approach.

3.1 First Principles Analysis of Flow within Wind Tunnel

The following section summarises how the first principles of fluid mechanics are applied to determine which components are required for this wind tunnel.

3.1.1 Study of Limiting Cases

An open-loop wind tunnel equipped with a pusher style fan leads to two limiting cases, which are 1) connecting the fan to the test section through a long duct to enable complete mixing and thus uniform test section inflow, or 2) attaching the fan directly to the test section to minimize the pressure rise required. While these limiting cases could provide simple solutions to the problem, the constraints are such that the former option is impractical due to the allocated room's length of 13.4 m. Considering the space that is needed for the test section there needs to be a limit on the length of duct between the fan outlet and the test section inlet. For the case of the fan being directly connected to the test section, a high flow non-uniformity is expected to enter the test section, as seen in Fig. 3-2.

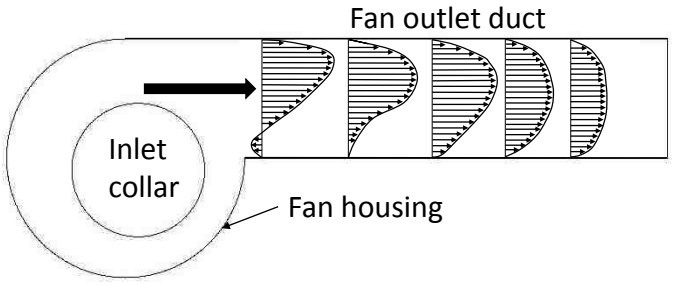

Figure 3-2: High flow non uniformity at fan outlet.

It is obvious that neither of the limiting cases is appropriate based on the constraints regarding space limitations and required flow uniformity. This leads to the conclusion that there is a need for a certain length of duct between the fan outlet

and the test section inlet. Since it is expected that the fan outlet and test section areas will differ, it can be established that some length of non-constant area duct is required.

3.1.2 Fan Selection

As suggested by Bradshaw[8], the volume flow rate and static pressure rise required to drive the air throughout the tunnel need to be defined to select a fan. With the maximum volume flow rate defined, the static pressure rise required to drive air throughout the wind tunnel is determined by estimating the total pressure loss for the wind tunnel and test section. The breakdown of the total pressure drop estimated for the wind tunnel is illustrated in Table 3.1. The total estimated loss is expressed in terms of the test section inlet dynamic pressure ($= \frac{1}{2}\rho(\bar{U}^X_{ts,i})^2 = 992$ Pa). Since the total pressure drop for the test section is not known, a conservative measure is taken by estimating it to be two times the test section inlet dynamic pressure. The exit dynamic pressure is simply based on the maximum possible test section inlet dynamic pressure; and the total pressure drop for the wind tunnel, as explained in section 1.2.2, is estimated to be one fan outlet dynamic pressure.

Table 3.1: Breakdown of estimated total pressure drop for wind tunnel system.

Factors	Estimated loss	Total pressure drop (Pa)
Test section	2 x Test section inlet dynamic pressure	1894
Exit dynamic pressure	1 x Test section inlet dynamic pressure	992
Wind tunnel allowance	1 x Fan outlet dynamic pressure	245
	Total	3185

The total pressure of 3185 Pa represents 3.25 times the test section inlet dynamic pressure. To account for any potential additional total pressure drop, a margin of ≈ 0.30 test section inlet dynamic pressure is added to this estimate, leading to a total estimated loss of 3484 Pa, which is approximately equal to 14 inWG. This pressure rise required from the fan coupled with the volumetric flow rate of 12.9 m^3/s are used to select a potential fan from the manufacturer Northern Blower. As suggested by Mehta [4] and Bradshaw [8], a centrifugal fan with airfoil-type blades is chosen. The performance curve of the 5730 fan design (size 3650) together with a simple sketch of the fan, provided by Northern Blower [28], is seen in Fig. 3-3. The selected fan provides the maximum volume flow rate of 12.9 m^3/s (27350 cubic feet per minute (CFM)) with an outlet velocity of $0.504\bar{U}^X_{ts,i}$ through an outlet of dimensions of w by $1.73w$, where $w = 0.613$ m.

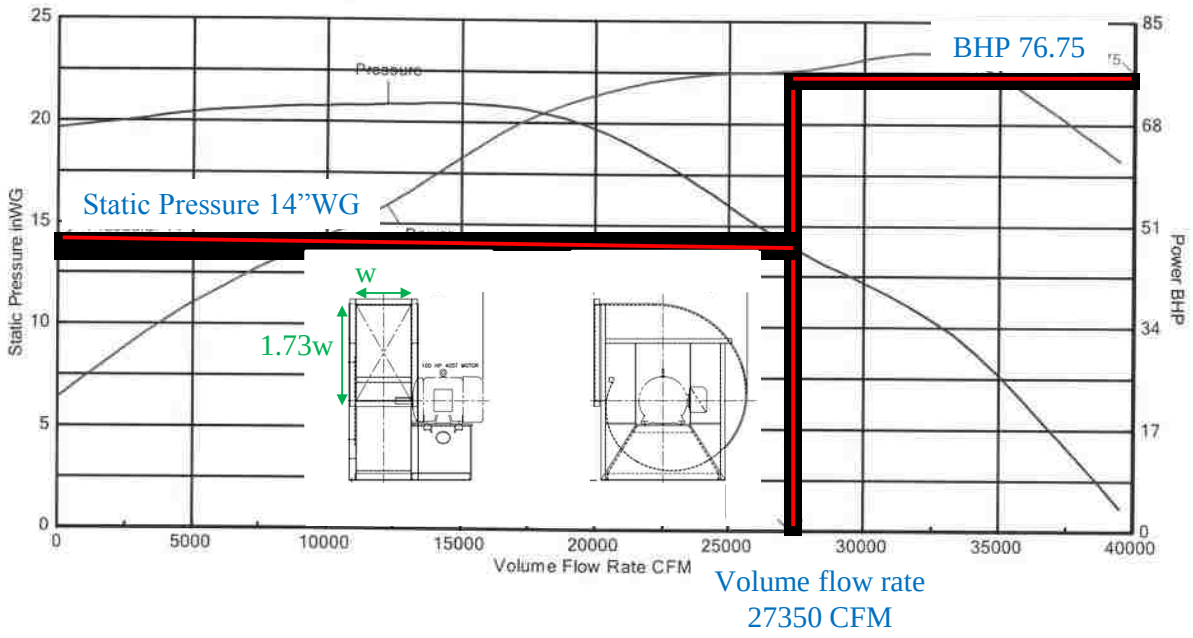

Figure 3-3: Centrifugal fan performance curves and outlet dimensions.

3.1.3 Fan Outlet Duct Requirement

As sketched in Fig. 3-2, the fan outflow is expected to exhibit high flow non-uniformity. To prevent the possibility of further increasing any losses in the downstream component, a duct with same dimensions as the fan outlet is attached downstream of the fan. Sugarman [29] indicates that for a fan outlet velocity of 12.7 m/s or less, the length of the duct downstream of the fan outlet should be 2.5 times the duct diameter with one added duct diameter for each additional 5.1 m/s in speed. With the selected fan, the outflow velocity is 20.1 m/s, implying the need for a duct of length equal to four times the duct diameter. The duct diameter, D, is calculated using Eq. 3.1 given by the Air Movement and Control Association (AMCA) handbook [30]. This diameter is that of a circular duct with equal area as the rectangular fan outlet.

$$D = \sqrt{\frac{4lw}{\pi}} \tag{3.1}$$

In this equation, l and w are the dimensions of the fan outlet. The required length of the duct is found to be $5.93w$, which is about 3.63 m, representing 46.7% of the allowable length of the tunnel or 27.1% of the room's length. Since there is a need for space to accommodate more components, used to change speed of the flow and allow mixing of the fluid flow before it reaches the test section, this length of duct is more than what can be used.

Referring to Fig. 3-2, as the duct length is increased, the outflow from the fan outlet approaches a fully developed state, comprising a symmetric velocity profile. Therefore, in determining the length of this fan outlet duct, the aim is not to reach the fully developed velocity profile but rather provide sufficient duct length to achieve a velocity profile which is at least near to symmetric. From the same figure, it is clear that the duct should be between 50% and 75% of the required length to achieve such a velocity profile. By considering the constraints and this factor, the maximum possible length of the duct is determined to be 66% of what is recommended, equal to $3.92w$.

3.1.4 Diffuser to Reduce Fan Outflow Velocity

Mixing of the flow from the fan outlet is required to achieve high flow uniformity, and as discussed in section 3.1.1, the viscous dissipation, associated with this process scales with the cube of the velocity. Therefore, to reduce the power required to overcome the dissipation associated with mixing, the process should take place at low speed. This means that a component with the ability to reduce the flow speed is required. As discussed by Mehta, it is common to use a diffuser, as seen in Fig. 3-4, to achieve such results [9]. With the diffuser stability map revolving around two-dimensional diffusers, a planar diffuser is envisioned for this wind tunnel.

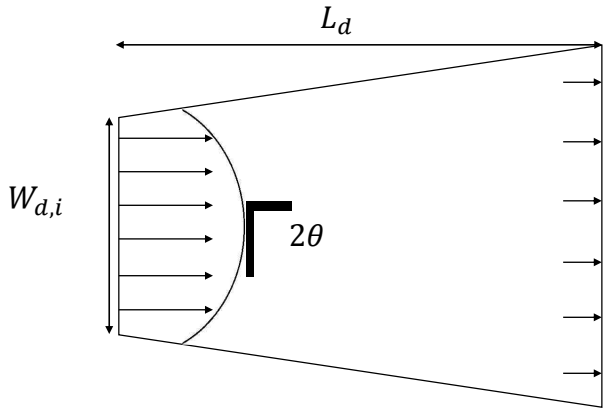

Figure 3-4: Diffuser to slow down flow.

To determine the fan dimension across which diffusion will be considered (w or $1.73w$), the "No Appreciable Stall" region of the diffuser stability map is used to ensure an analysis based on a diffuser with no flow separation. For each of the two dimensions of the fan outlet, the ratio of $\frac{L_d}{W_{d,i}}$ is calculated, and the corresponding diffusion angles are obtained from the graph. It is determined that by expanding the duct across the shorter side, w, a larger area ratio, hence a lower flow velocity, is obtained.

While a diffuser is critical to allow mixing at low speed, it is at risk of two fluid flow phenomenon. Given by equation 3.2, the velocity of a flow within a diffuser depends on its acceleration and the pressure gradient across it. In the presence of flow non-uniformity, as seen from the left side of Fig. 3-5, with an increasing cross-sectional area in the streamwise direction, the flow slows down. For the same pressure gradient across the duct, slow flow has a larger deceleration $\frac{du}{dx}$, causing the speed of the slow flow to drop at a faster rate while the speed of the faster flow reduces at a slower rate. Therefore, this flow behaviour accentuates the difference between the two flows.

$$u\frac{du}{dx} = \frac{1}{\rho}\frac{dp}{dx} \tag{3.2}$$

The other concern with a diffuser is flow separation. In any flow, the flow near the wall travels at a slower speed, and thus can easily be affected by the adverse pressure gradient in a diffuser. When this pressure gradient is large enough, the fluid may show down to a zero velocity away from the wall or even become reversed. As seen in the right part of Fig. 3-5, this leads to flow separation.

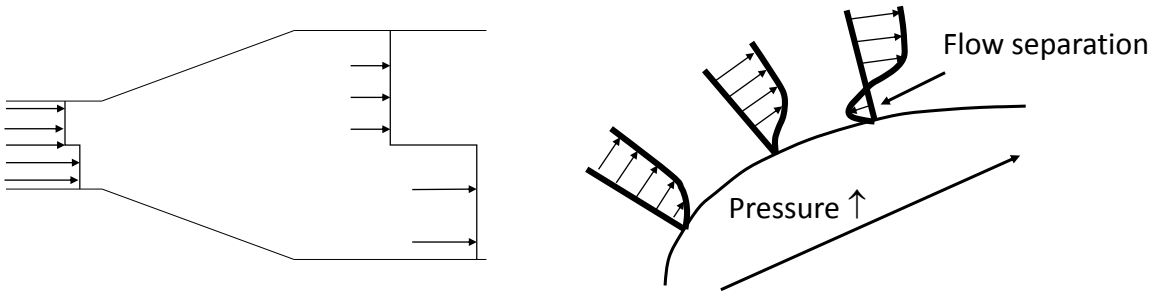

Figure 3-5: Flow field within a diffuser. Left: flow non-uniformity accentuates; right: onset of flow separation.

Analysis of the first principles of fluid mechanics enables the determination of which component is required downstream of the fan attached to the constant area duct; however, further investigation is required to determine the best dimensions for this diffuser. Therefore, to determine the length, coupled with the diffusion angle, two-dimensional CFD computations are required, as described later.

3.1.5 Flow Straightener to Reduce Secondary Flows

For the ideal case of a diffuser with diffusion angle of no more than 20° (no flow separation), mixing of the flow would require a long duct, making it more challenging to respect the compact requirement of this project. In the presence of amplified flow

non-uniformities due to flow separation, mixing enhancement required within a short distance can be achieved via a flow straightener.

As discussed by Barlow and Cattafest et al. [6, 7], a honeycomb is used to align the flow with the axis of the tunnel and to reduce secondary flows by breaking up large scale flow unsteadiness. This honeycomb is envisioned to comprise hexagonal cells due to its popularity with regards to low pressure drop.

Downstream of the honeycomb, a constant area duct is required to further break the small scale unsteadiness through the mixing of the jets and wakes. There is a restriction on the length of this duct due to boundary layer development. Screens within the flow straightener section are omitted due to the challenge of obtaining rigid ones for the large cross-sectional area.

Two-dimensional CFD calculations are required to determine the length of the flow straightener section for this wind tunnel. Further investigations are needed to establish the cell size of the honeycomb, as well as the length of the structure.

3.1.6 Nozzle Reducing Flow Non-Uniformity Entering Test Section

To connect the large cross sectional area of the flow straightener to that of the test section, a nozzle is needed to accelerate the flow to its design speed. In a nozzle, due to the decrease in cross-sectional area, the flow speed increases and there is a favourable pressure gradient. In the presence of a flow non-uniformity, as seen in the left side of Fig. 3-6, the speed of the slow flow increases at a higher rate than the speed of the fast flow. Therefore, the difference between the two flows reduces, leading to a lower flow non-uniformity. Also, due to the favourable pressure gradient within the nozzle, the velocity profile gets flatter near the wall. As shown in Fig. 3-6 on the right, this further reduces the flow non-uniformity.

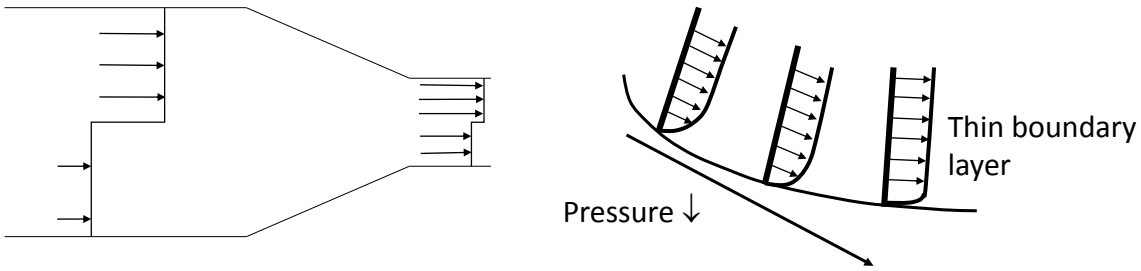

Figure 3-6: Flow field within a nozzle. Left: flow non-uniformity decreases; right: flattened velocity profile near wall.

For this wind tunnel, two nozzles are required to accommodate circular and rectangular cross-section test sections, as seen in Fig. 3-7, with both having the same outlet area. With respect to the nozzle design, the length is constrained with the space taken by the diffuser and flow conditioner. One-dimensional analysis of the nozzle cannot capture flow non-uniformity introduced due to wall curvature in an aggressive nozzle. Therefore, a parametric study of 2D CFD computations is carried out to determine the shortest length with acceptable flow non-uniformity. The results of this study will be presented in section 4.2.

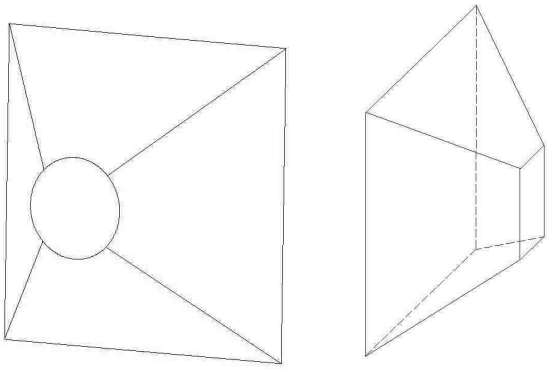

Figure 3-7: Geometry of two nozzles required.

3.1.7 Summary of First Principles Analysis

From this analysis, a high-level design of the wind tunnel is established. The schematic of the wind tunnel, as seen in Fig. 3-8, comprises a constant area duct which connects the fan to the diffuser, followed by a honeycomb coupled with a mixing chamber. The wind tunnel ends with a nozzle to accelerate the fluid from the flow straightener to the test section.

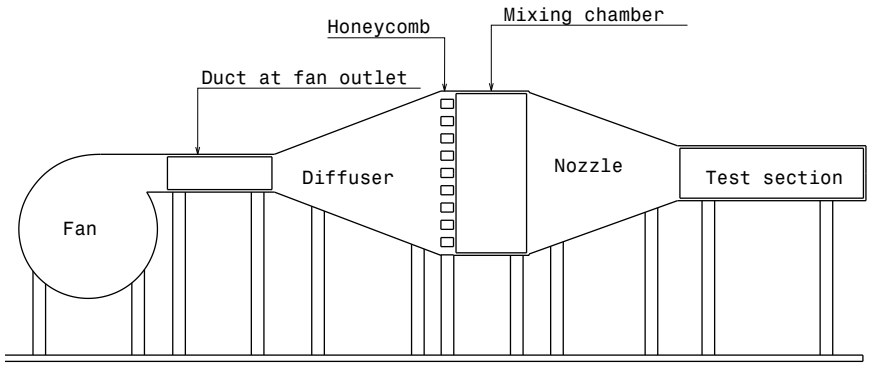

Figure 3-8: Design concept based on first principles analysis.

3.2 Two-Dimensional Computational Fluid Dynamics Analysis of Wind Tunnel

Based on the design concept obtained from the first principles analysis, a parametric study of each of the components is required to determine a wind tunnel design which satisfies the loss coefficient and flow non-uniformity constraints. With the exception of the duct downstream of the fan, all the other components' lengths, radii of curvature (if any) and other dimensions are varied individually and investigated, as described in this section. To keep the scale of the parametric study practical, component designs are finalized one by one from upstream to downstream.

3.2.1 Diffuser

With a planar diffuser considered for this wind tunnel design, its outlet dimension is set to reach the constraint of 2m to achieve the minimum flow speed. With the inlet and outlet set, according to the diffuser stability map given by Reneau et al. [10], the parameter investigated is its length, mainly due to the compact requirement of this project. To respect the overall tunnel length constraint, the maximum diffuser length investigated is $4.1w$, yielding a diffusion angle of 31°. The diffuser stability map indicates that with this maximum length, the diffuser flow will be well within the transitory stall regime; therefore, as seen from Fig. 3-9 a flow separation bubble fluctuates between the two diffusing sides.

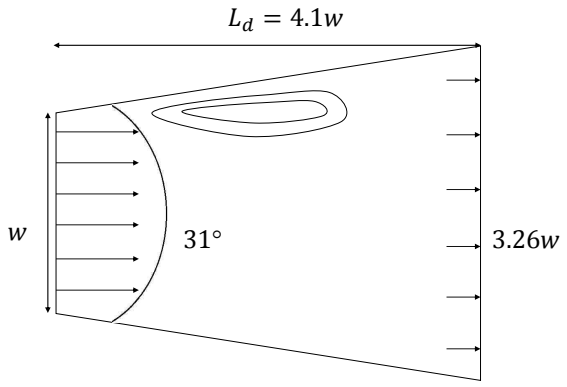

Figure 3-9: Flow separation for upper limit of diffuser length.

As discussed in section 2.3.2, a boundary layer control mechanism is required to prevent flow separation; in this case, the use of screens within the diffuser is investigated. The use of this boundary layer control mechanism imposes a limit of $2.9w$ as the minimum length of diffuser. With a shorter diffuser, the screens are insufficient to tackle the problem of flow separation as the diffusion angle being more than 55°, as indicated by Mehta [4], leads to the "bistable steady stall" region of the diffuser stability map given by Reneau et al. [10]. To determine the right combination of screens for this application, the number of screens is parametrically varied from 0

to 3 and their locations are varied along the diffuser length, with the original positions being the same as in the work of Noui-Mehidi [17]. From the given locations of screens, the positions of the screens are then varied by increments of 1% of the diffuser length until the best locations to reach a balance between the loss coefficient and the flow non-uniformity are determined. The presence of screens are modelled computationally as porous jumps with a 50% solidity ratio.

3.2.2 Flow Straightener

When investigating the flow straightener design, the cases with and without a honeycomb are considered. The honeycomb is modelled as a series of parallel, zero thickness plates in the two-dimensional computations. To achieve a ratio of length of honeycomb element to hydraulic diameter close to the minimum requirement outlined by Barlow [6], an initial estimated cell size of $0.0653w$ coupled with the upper limit of $0.326w$ as the length of the honeycomb is investigated. Any increase in this length is restricted by the space constraints imposed on the wind tunnel design. To determine whether a 50% decrease in the aforementioned ratio would affect the flow non-uniformity and loss coefficient, a $0.163w$ long honeycomb is also investigated. The lower limit of the study of the impact of honeycomb cell size, which is a common size for honeycomb panels, provides a comparison between two honeycombs having a 60% difference in dimensions.

To determine the point where boundary layer development starts to dominate within the mixing chamber (the point at which the flow non-uniformity reaches a minimum) a $5w$ long constant-area duct is modelled downstream of the honeycomb.

3.2.3 Nozzle

An upper limit of $3.10w$ is chosen for the assessment of the nozzle length based on the overall size constraints for the tunnel. By reducing the length of the nozzle by

$0.240w$ in steps, the most compact nozzle design respecting the limits imposed on the figures of merit is achieved.

Supporting the discussions made by Mehta and Bradshaw, and Morel [4, 20], the nozzle is envisioned with smooth arcs at both the inlet and outlet of the nozzle joining the parallel sections such that the first and second derivatives of the curve at the connecting point is zero. While it is suggested that the nozzle's contour is comprised solely of these two curves, this investigation is carried out with the two curves being connected by a straight line, as illustrated in Fig. 3-10. This feature is included to simplify manufacturing, especially for the circular nozzle. The radii are both gradually increased by $0.16w$ to obtain as close to "two cubic arcs joined smoothly" as possible, as discussed in section 2.3.4.

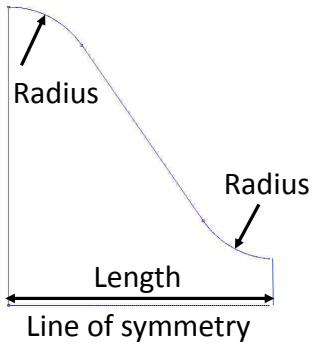

Figure 3-10: Radii of curvature at nozzle inlet and outlet.

3.2.4 Numerical Setup

To predict the flow field within the wind tunnel, ANSYS Fluent 17.0 is used [31]. With a steady pressure-based solver, the Semi-Implicit Method for Pressure-Linked Equations (SIMPLE) is adopted as the velocity-pressure coupling method. Due to the lack of information regarding the velocity profile at the fan outflow, the inlet boundary is set as a constant-area duct upstream of the diffuser inlet to decouple the imposed uniform inlet velocity of $0.5\bar{U}^X_{ts,i}$ from the diffuser wall curvature. The turbulence

intensity at the inlet is set to 1% and the length scale is the inlet hydraulic diameter, and all walls are assumed to be smooth. This assumption is considered acceptable as any actual flow non-uniformity will be attenuated by the screens within the diffuser. A pressure outlet boundary is used to set the stagnation pressure level. The Reynolds number based on test section inlet velocity, $\bar{U}^X_{ts,i}$, and hydraulic diameter, $1.05w$, is 2×10^6. Based on the study carried out by Bardina et al. [21, 22], the SST model given by Menter is used in steady Reynolds-Averaged Navier-Stokes (RANS) computations since some flow separation is expected . The specifications of the porous jump is as seen in Table 3.2.

Table 3.2: Porous jump specifications.

Face permeability (m^2)	1×10^{10}
Porous medium thickness (m)	1
Pressure-jump coefficient, C2 (1/m)	2

As discussed by Moonen [26], the grid is made of both structured mesh, in the honeycomb section and the boundary layers, and unstructured mesh in all other sections, to avoid expensive computations. To ensure a good quality grid is obtained, mesh parameters such as orthogonal quality and skewness are checked to be within the respective ranges of 0-1 (best when closer to 1), and less than 0.5 (best when closer to 0), respectively as outlined by ANSYS Help 17.0. The structured mesh present in the boundary layer is defined by a maximum y^+ of 60, and the end-wall boundary layers are resolved with 10 cells.

As indicated in Table 3.3, flow solutions obtained on three grids, comprising between 75,000 and 251,345 cells showed that grid independence is obtained for a grid with 136,175 cells. The key metrics of concern are the flow non-uniformity and the loss coefficient at the nozzle outlet. The simulations are treated as converged when

the mass flow rate, the total pressure, and the velocity at the diffuser inlet, at the nozzle inlet, and at the nozzle outlet change by no more than 1%.

Table 3.3: Percentage change in $RMS\%$ at nozzle outlet relative to grid with 75,000 cells.

Number of cells	136,175	251,345
% Change in cell size	50	67
% Change in $RMS\%$	0.15	0.69

3.2.5 Limitation of Two-Dimensional CFD Computations

While the two-dimensional calculations allow the sizing of the different components, some factors are overlooked in this process. These are: 1) 3D relief effects; 2) the side end walls, which are not considered, provide higher friction, and thus lead to an increase in total pressure drop; and 3) the honeycomb elements comprising six walls instead of two, as modelled in the two-dimensional CFD calculations, also contribute to higher total pressure drop. Hence, since two-dimensional CFD is insufficient to quantify the additional expected loss, three-dimensional CFD calculations are required to provide a more accurate estimation of the total pressure drop and the flow non-uniformity.

3.3 Three-Dimensional Computational Fluid Dynamic Analysis of Wind Tunnel

The model used for the advanced numerical calculations is based on the final design obtained from two-dimensional calculations. A quarter of the wind tunnel design, as seen in Fig. 3-11, is modelled due to its symmetry along the vertical and

horizontal planes. The setup used for the three-dimensional CFD is similar to the two-dimensional one, with the use of a pressure-based solver in ANSYS Fluent 17.0. Using the same velocity pressure coupling (SIMPLE), the SST turbulence model, and the boundary conditions duplicated from the two-dimensional CFD setup, a steady three-dimensional model is analyzed.

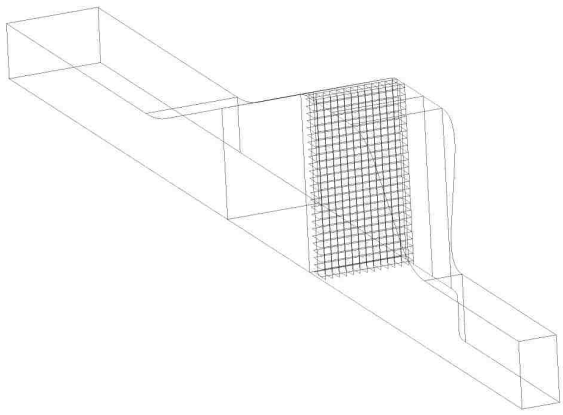

Figure 3-11: Quarter 3D model.

The grid is made of regions of structured and unstructured mesh matching those in the two-dimensional setup and consists of 16,873,210 cells. While the screens are still represented by porous jumps, the honeycomb structure is created by modelling vertical and horizontal walls to create the sides of each honeycomb element. This still represents a simplification of the honeycomb structure which allows for a less intricate grid requiring less time to set up. Using three-dimensional CFD, it is also possible to model the flow field for the case when the tunnel is attached to the rectangular nozzle as well as when the circular nozzle is mounted, providing a more accurate prediction of the flow characteristics for each instance. The same convergence requirements are set for the three-dimensional CFD simulations, with the key metrics of concern remaining the same as in the two-dimensional CFD case.

3.4 Summary of Approach

From the three-dimensional CFD simulations, a better estimate of the loss coefficient and $RMS\%$ is obtained, thus making it possible to determine whether the potential fan, outlined in section 3.1.2, provides sufficient pressure rise for this wind tunnel design. In the case where the potential fan is successful, the assembly design, as discussed in chapter 5, will be created and the manufacturing phase will be started. However, if the potential fan is insufficient for this application, another fan with a higher static pressure rating will selected. This would be followed by the repetition of all other steps outlined in this chapter, except for the analysis based on first principles, to yield an appropriate design respecting the constraints set. This iterative process is not only applicable to wind tunnels but also other internal fluid flow systems, where the analysis based on first principles is performed to identify the different components required before sizing them using two-dimensional CFD calculations, and obtaining more accurate results with three-dimensional CFD calculations. In completing this project, this iteration process is not actually required.

Chapter 4

Results

The discussion of the results of two-dimensional and three-dimensional CFD calculations show how successful the outlined approach is for modelling this wind tunnel. This chapter presents the final wind tunnel design that is obtained using the approach discussed in Chapter 3.

4.1 Overview of Final Wind Tunnel Design

Following the approach outlined in this thesis, the final wind tunnel design, as seen in Figs. 4-1 and 4-2, is obtained. This wind tunnel assembly comprises a $3.9w$ long constant area duct followed by a $3.6w$ long wide-angle diffuser, with a diffusion angle of 37.8°, with two screens separating it into three sections. The two screens, each with a 50% solidity ratio, are located at $1.7w$ and $3.2w$ from the diffuser inlet, representing 47.5% and 90% of the diffuser length respectively. The flow straightener section comprises a honeycomb structure of length $0.16w$ with cell size of dimension $0.041w$ attached to a $0.82w$ long mixing chamber. Both nozzles measure $1.5w$ in length, and connect the $3.3w$ by $1.73w$ cross section of the mixing chamber to the respective test section inlets of area 0.326 m^2. The curves smoothing the flow from the mixing chamber and into the test section have radii of $0.65w$.

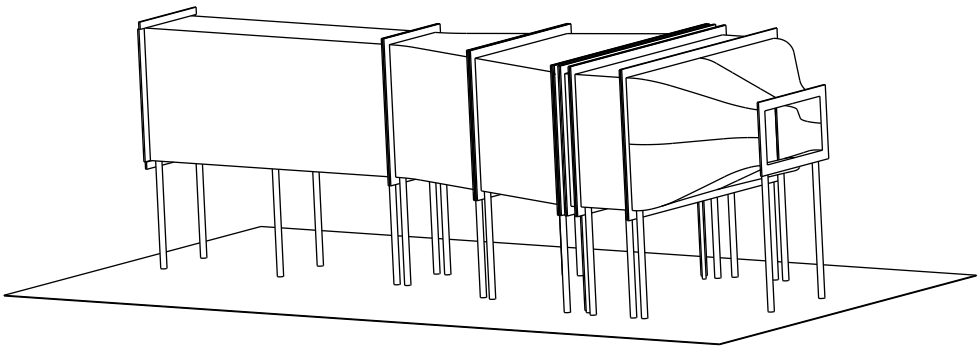

Figure 4-1: Wind tunnel assembly with the rectangular nozzle attached.

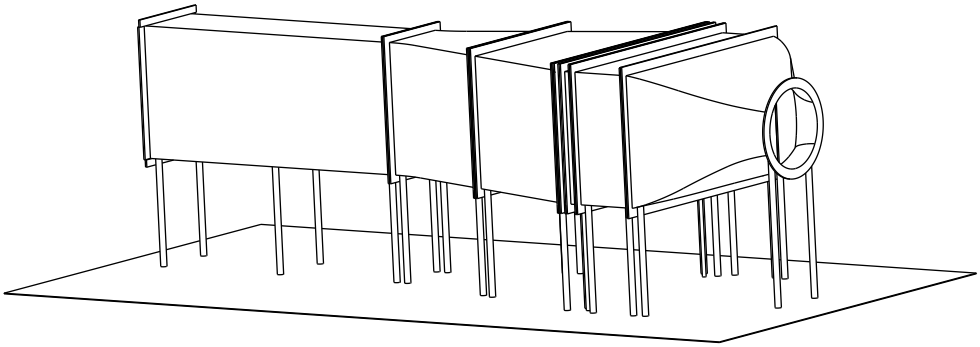

Figure 4-2: Wind tunnel assembly with the circular nozzle attached.

4.2 Results of Parametric Study

In this section the results of the parametric variation of the geometry of each tunnel component is detailed.

4.2.1 Diffuser Length

By analysing the key metrics at the diffuser outlet, it is observed that without screens within the diffuser, a $4.1w$ long diffuser leads to high flow non-uniformity represented by an $RMS\%$ value of 74.9%. A 28% decrease in length, leading to the lower limit of a $2.9w$ long diffuser, leads to higher flow non-uniformity given by a $RMS\%$ value of 80.7%. This shows that a more aggressive diffuser leads to higher flow non-uniformity.

While both diffusers yield loss coefficients less than 0.1, a $4.1w$ long diffuser is initially selected to further the investigation as it is expected that the flow non-uniformity together with the loss coefficient would increase when the three-dimensional CFD is carried out. The reason underlying the expected increase in loss coefficient is due to the added friction caused by the side end walls; the positive pressure gradient is expected to enhance the flow non-uniformity in the three-dimensional CFD calculations. It is especially critical to provide some margin in the case of a positive pressure gradient duct such as a diffuser. Further, as mentioned in section 3.2, the parametric study is performed by starting with the upstream component before proceeding to the next one; therefore, this decision is taken to remain conservative with respect to potential flow non-uniformity and losses downstream of the wind tunnel. Simulations of the wind tunnel with all sized components show that a 13.6% more compact diffuser provides an increase of 0.5% in $RMS\%$, and a rise of 5.67% in ω. This intermediate value of $3.6w$ helps maintain the compact requirement while still enabling flow re-attachment using screens and thus keeping the loss coefficient for the tunnel below the allowable upper limit.

4.2.2 Number of Screens Required

As seen from the high $RMS\%$ values obtained for diffusers without screens and by the velocity magnitude contours of Fig. 4-3, the presence of screens is critical to prevent flow separation and increase flow uniformity at the diffuser outlet. As indicated by Table 4.1, the use of two screens is the best option to reduce the flow non-uniformity while maintaining an acceptable total pressure drop.

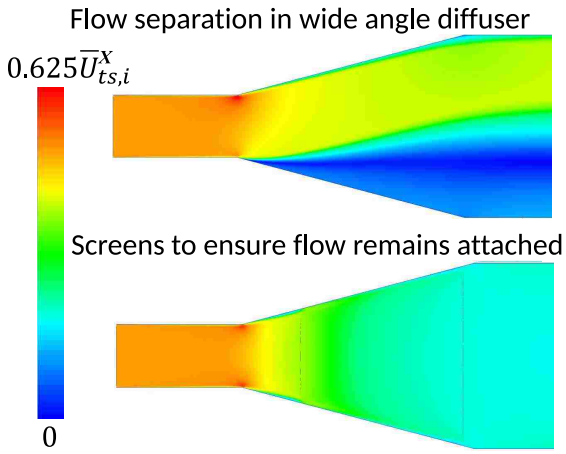

Figure 4-3: Impact of screens on flow in a wide-angle diffuser. Top: flow separation with no screens; bottom: attached flow due to presence of screens.

With one screen located beyond 50% of the diffuser length, either the flow cannot be re-attached further downstream, or the flow starts to separate again even after getting mixed downstream of the screen. Two cases with different a number of screens in a $4.1w$ long diffuser provide results as given in Table 4.1. The locations of these screens are given in Fig. 4-4. For the case of two screens, these are located at $0.25L_d$ and $0.95L_d$ and the position of the three screens are at $0.25L_d$, $0.59L_d$ and $0.95L_d$.

The results indicate that the addition of a third screen in between those at the ends leads to an increase of 1% in $RMS\%$. The local total pressure drop, as a result of the screen located at $0.25L_d$, leads to a favourable pressure gradient. This prevents the flow's tendency, near the wall, to go in the reverse direction; thus, ensuring that the flow remains attached. The energisation of the boundary layers following the first screen is sufficient to maintain attached flow between the first and second screens. When the flow reaches the screen positioned at $0.95L_d$, through the same mechanisms it prevents the flow from separating prior to leaving the diffuser.

The presence of an additional screen situated at $0.59L_d$ does not provide a benefit to flow uniformity since the flow after the first screen is attached and in fact yields a

higher $RMS\%$ at the diffuser outlet. Further, the presence of this screen occupying a larger cross-sectional area than the first screen represents additional resistance to the airflow; thus leading to an increase of 36.6% in loss coefficient. The addition of a third screen does not improve the flow quality. This leads to the conclusion that the implementation of two screens is the best option for this wind tunnel design.

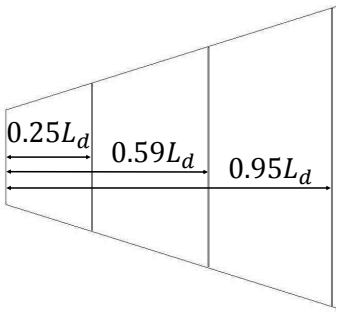

Figure 4-4: Location for analysis about required number of screens.

Table 4.1: Figures of merit for 2 vs. 3 screens.

Screen locations	$0.25L_d$&$0.95L_d$	$0.25L_d$, $0.59L_d$, and$0.95L_d$
$RMS\%$	10.4	11.3
ω (diffuser)	0.351	0.480

4.2.3 Location of Screens

To determine how much the flow non-uniformity can be decreased, the first screen is incrementally relocated downstream of the original position. As seen from Table 4.2, the best location of this screen is found to be at $0.475L_d$. Compared to the original location for two screens, as shown in Table 4.1, this pair of screens lead to a 42% decrease in loss coefficient, with a full 1% decrease in $RMS\%$.

Moving the first screen further downstream, with 1% L_d changes, displays neg-

ligible differences in flow non-uniformity since the screen still yields attached flow downstream. The $RMS\%$ begins to increase at $0.500L_d$ (at the fourth significant figure) indicating that the inflow non-uniformity is becoming more severe. Since a negligible difference is observed in the $RMS\%$ value for different first screen locations, it can be concluded that the location of this screen does not strongly influence its ability to re-energize the boundary layer.

Yet, this relocation of the screen to $0.475L_d$ from the diffuser inlet, where the loss coefficient reduces by 42%, reaffirms how lower total pressure drop can be achieved when mixing occurs at lower speed. When the screen is located at $0.590L_d$, the loss coefficient starts to increase again. This increase in loss is due to two factors: 1) a larger cross-sectional area with increased blockage, which increases the resistance against the flow and 2) the presence of a more developed separation bubble when the screen is moved at $0.590L_d$. With a higher blockage area, the flow has to undergo more resistance and hence a higher total pressure drop results. With a larger separation bubble, as seen from Fig. 4-5, there is a larger area in which the flow is going in a reverse direction, thus increasing the resistance to the flow.

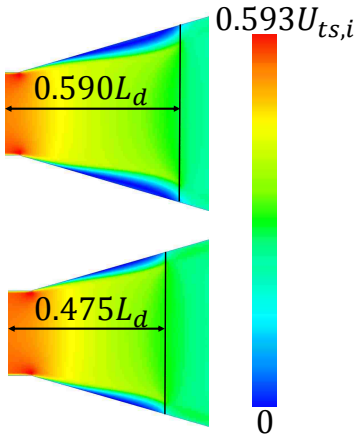

Figure 4-5: Larger separation bubble with screen located at $0.590L_d$.

Table 4.2: Impact of varying the first screen location; second screen at $0.95L_d$.

First screen location	ω	$RMS\%$
$0.280L_d$	0.331	10.415
$0.330L_d$	0.302	10.389
$0.380L_d$	0.281	10.370
$0.400L_d$	0.274	10.363
$0.450L_d$	0.257	10.351
$0.475L_d$	0.249	10.349
$0.500L_d$	0.243	10.349
$0.525L_d$	0.237	10.353
$0.550L_d$	0.232	10.358
$0.590L_d$	0.254	10.371

The same analysis applies to the location of the second screen; its relocation to $0.9L_d$ reduces the distance between the two screens, hence contributing to a 0.2% rise in $RMS\%$. Due to the smaller cross-sectional area at this location, flow mixes at a higher speed leading to a 1.65% higher total pressure loss coefficient. However, since these changes are negligible and to ensure manufacturability of the diffuser, the second screen is kept at $0.9L_d$.

4.2.4 Flow Straightener

As seen in Fig. 4-6, the presence of a honeycomb leads to a 2.52% higher $RMS\%$ within $0.163w$ from the diffuser outlet. This difference in $RMS\%$ is mainly due to the mixing process occurring; the lower flow non-uniformity, in the absence of a honeycomb structure, indicates that the flow from the second screen within the diffuser is getting mixed. However, this key metric rises and stabilizes after an increase of 5%, marking the end of the mixing process.

The presence of a honeycomb, comprising 50 elements of cell size $0.0653w$, downstream of the diffuser causes this metric to decrease to a minimum within $0.816w$ from the diffuser outlet before increasing again. This indicates that the flow non-uniformity is driven by two mechanisms: 1) the evolution of the end wall boundary layers and 2) the velocity non-uniformity far from the end walls caused by the upstream diffuser flow. The former tends to increase the non-uniformity as the flow moves downstream while the latter decreases as the flow mixes out. Hence, when the initial (post-honeycomb) non-uniformity is sufficiently low, a location of minimum flow non-uniformity exists.

Thus, the mixing length past the honeycomb is kept to only $0.816w$ to aid in maintaining the compact requirement. Further, Fig. 4-6 indicates that the presence of a honeycomb reduces the mixing length required downstream of a diffuser, thus reaffirming the need for this structure. It is understood that these results will alter due to the presence of the nozzle; yet, to keep the scope manageable, only one component was investigated at a time.

Computations show that at this location of minimum flow non-uniformity, a 50% decrease in the honeycomb length leads to an increase of $4 \times 10^{-3}\%$ in $RMS\%$, and to a $8 \times 10^{-4}\%$ higher loss coefficient. Therefore, to provide a compact design of the honeycomb structure, all while trying to remain close to the range of length to hydraulic diameter suggested by Barlow [6], a $0.163w$ long honeycomb is adopted.

Further, a 36.5% decrease in honeycomb cell size causes a reduction of only 1.3×10^{-2}% in flow non-uniformity while causing an increase of 2.9% in the loss coefficient. While this indicates that a smaller cell size is more effective in breaking down the large scale unsteadiness from the diffuser, it also shows that a smaller cell size leads to higher friction due to the added wall surface area. With negligible changes in the key metrics as the cell size is decreased, a honeycomb with a cell size of $0.0414w$ is selected. This decision is also based on the fact that this is the usual maximum honeycomb cell size, and any larger sizes would lead to higher costs.

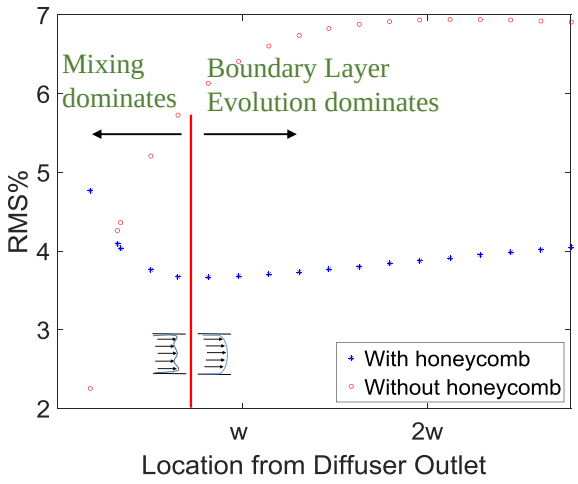

Figure 4-6: Impact of honeycomb on $RMS\%$ downstream.

4.2.5 Nozzle

Decreasing the length of a nozzle by up to 52.6% leads to a drop of 0.12% in loss coefficient due to the shorter length of the nozzle. The flow non-uniformity increases by 0.2% due to the aggressive nature of the nozzle. This complies with the findings made by Morel [20] indicating that a long nozzle is desired to avoid flow separation at the nozzle outlet. Fig. 4-7, showing the velocity profiles for the two limiting cases, demonstrates that a longer nozzle is desired for lower flow non-uniformity; yet for this case, the difference between the two profiles and the figures of merit are negligible.

Since a further decrease of 16.7% in length, from the lower limit, leads to a a 0.3% and 0.12% rise in $RMS\%$ and ω, respectively, a $1.47w$ long nozzle is adopted for this wind tunnel design. This choice of length allows a more compact nozzle to be implemented while providing enough margin for any additional total pressure drop and flow non-uniformity that may arise in the three-dimensional case.

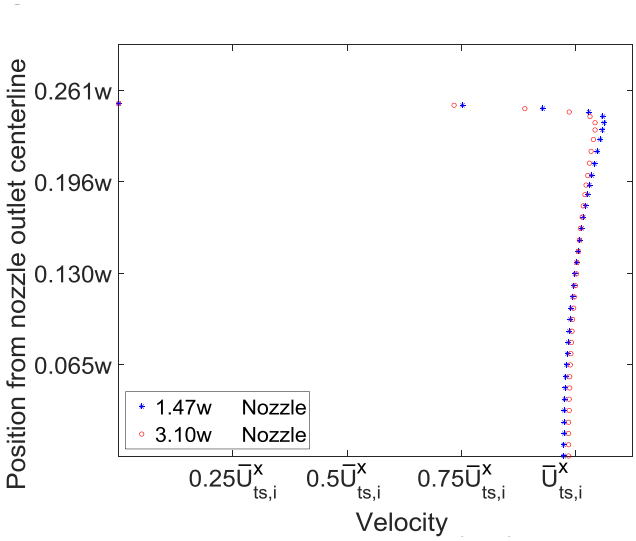

Figure 4-7: Test section inlet velocity profiles.

Adding curvature to the nozzle walls helps to decrease the flow non-uniformity at nozzle exit. Analysis of the radii of curvature at the inlet and outlet of the nozzle indicates that a largest possible radius should be maintained to ensure better flow uniformity. The largest radius possible, all while maintaining zero value of first and second derivatives of the curve at the nozzle inlet and outlet, is determined to be $0.653w$. With this radius at both the upstream and downstream ends of the nozzle, a $RMS\%$ of 5.84% and tunnel loss coefficient of 0.244 are achieved. As the radii are reduced to $0.490w$, both $RMS\%$ and ω increase by 0.21% and 0.12% respectively. Thus, the radii are kept at the maximum possible value.

4.2.6 Summary of Two-Dimensional Results

As seen from Fig. 4-8, two-dimensional CFD computations are successful in capturing the flow behaviour in the different components. As the flow enters the diffuser, the speed decreases; the onset of flow separation, as expected, is attenuated by the presence of the first screen. The flow field downstream of the honeycomb illustrates regions of jets and wakes which get mixed out before entering the nozzle. As the flow enters the nozzle, the flow speed increases to reach a maximum at the nozzle outlet.

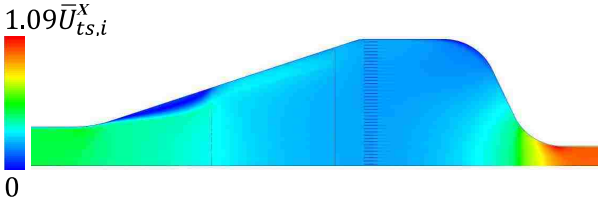

Figure 4-8: Velocity field for selected configuration in 2D CFD.

Results indicate that a longer diffuser is beneficial in terms of lower loss coefficient and reduced flow non-uniformity. A 40% longer diffuser leads to a drop of 14.5% in loss coefficient with 5.81% lower $RMS\%$. CFD results re-affirm the need for screens within wide angle diffusers to prevent the onset of flow separation with a 64% drop in $RMS\%$ with two screens. The screens, located at 47.5% and 90% of the diffuser length, ensure the boundary layers remain attached to the walls of the wind tunnel.

These computations also demonstrate that the presence of a honeycomb structure not only reduces the flow non-uniformity downstream of the diffuser, but it also reduces the mixing length required before the nozzle inlet. Further, a longer honeycomb, increasing the length to hydraulic diameter ratio, improves the fluid flow by reducing the flow non-uniformity and leading to a lower total pressure drop. It is shown that a smaller cell size of the honeycomb structure leads to a higher loss coefficient due to the additional skin friction.

While this wind tunnel design aims at the most compact nozzle possible, to meet

the set requirements, and to account for any additional non-uniformity and total pressure drop not accounted for in this two-dimensional calculations, results show that the longer the nozzle is, the better the flow conditions at the outlet are. This is further enhanced with the largest possible radii of curvature, with zero value of first and second derivatives of the curve at the meeting points with the mixing chamber outlet and the test section inlet.

Two-dimensional simulations conclude with a sized wind tunnel exceeding performance requirements, and satisfying the geometric constraints. The computations indicate that the flow non-uniformity at the outlet of the wind tunnel is estimated to be 5.84% with a loss coefficient of 0.218. This provides sufficient margin to proceed to the three-dimensional CFD calculations.

4.3 Results of Three-Dimensional CFD Calculations of Wind Tunnel

Fig. 4-9 demonstrates how fluid flow behaviour, predicted in a two-dimensional CFD computation, qualitatively matches those obtained with the detailed three-dimensional numerical calculations. The most obvious difference is that the separation within the diffuser is accentuated in both the 3D rectangular and the 3D circular cases. It is also observed that by the mixing chamber, the flow field is similar in all three cases.

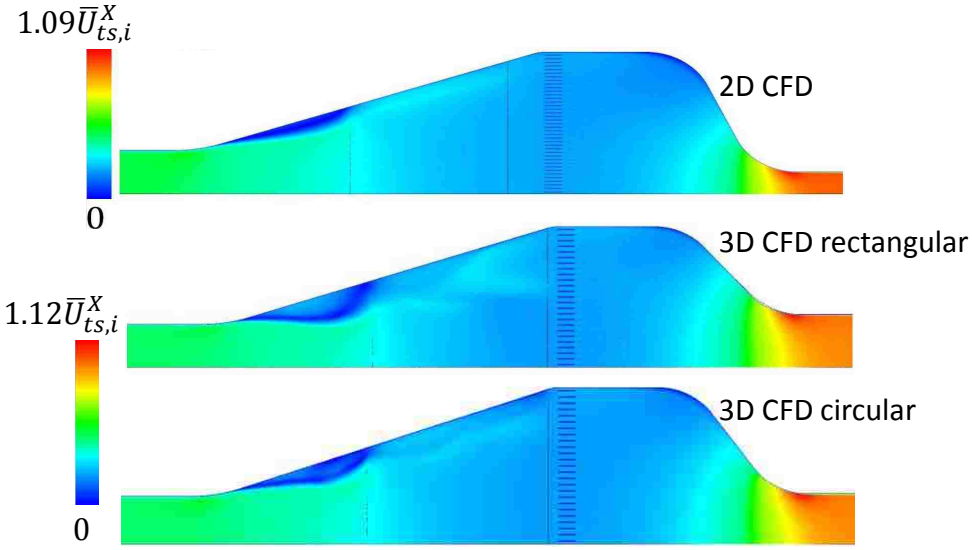

Figure 4-9: Velocity field for selected configuration in 2D CFD and 3D CFD.

While the overall behaviour is found to be similar, the same cannot be said about the quantitative values of loss coefficient and flow non-uniformity. Table 4.3 show that the $RMS\%$ value increases from 5.84% to 8.07% (with a rectangular nozzle exit), and 6.08% (with a circular nozzle exit), while the loss coefficient increases by 6% from what is obtained in the 2D computations. The increase in the figures of merit is expected since the two-dimensional CFD calculations fail to account for the skin friction on the sidewalls and underestimate the losses through the honeycomb (due to increased wall area and thus skin friction present in the three-dimensional model).

Table 4.3: Comparisons of figures of merit at the nozzle outlet.

Figures of merit	$RMS\%$	ω
Two-dimensional	5.84	0.224
Three-dimensional (circular nozzle)	6.08	0.225
Three-dimensional (rectangular nozzle)	8.07	0.238

The increase in the figures of merit is supported by Fig. 4-10, which illustrates the velocity variation on the nozzle outlet cross-section in the three-dimensional case. Compared to the two-dimensional model, the three-dimensional ones present a velocity gradient over a longer surface area. In the case of the rectangular nozzle, the flow non-uniformity is higher than with the circular one because of a more severe velocity gradient at the corner where the boundary layers on the two sides meet. This difference in figures of merit between the two-dimensional and three-dimensional case may also be due to the change in geometry along the nozzle, a complex aspect of the nozzle which is not captured by two-dimensional CFD calculations.

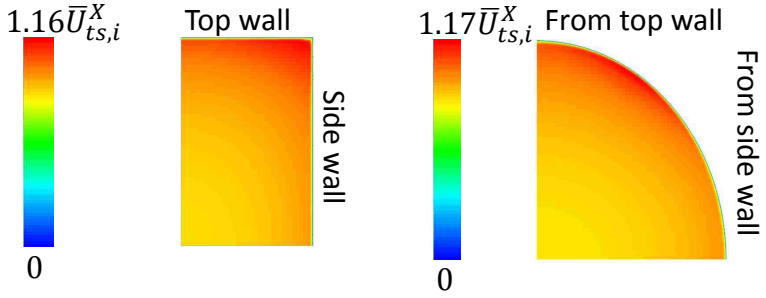

Figure 4-10: Nozzle outlet velocity contours for 3D cases.

Figs. 4-11 and 4-12 depict the stream wise evolution of the $RMS\%$ and ω, respectively, for the two-dimensional and three-dimensional simulations. The locations

denoted as $'f, o'$, $'d, i'$, $'s1'$, $'s2'$, $'h, o'$, $'n, i'$, and $'n, o'$, represent the locations of the fan outlet, the diffuser inlet, the first screen, the second screen, the honeycomb outlet, the nozzle inlet, and the nozzle outlet. Only in regions where mixing and/or flow separation are significant (in the diffuser and just downstream of the honeycomb) are the three-dimensional results markedly different from those obtained with the two-dimensional computations, aside from an overall increase owing to the higher skin friction in the three-dimensional case.

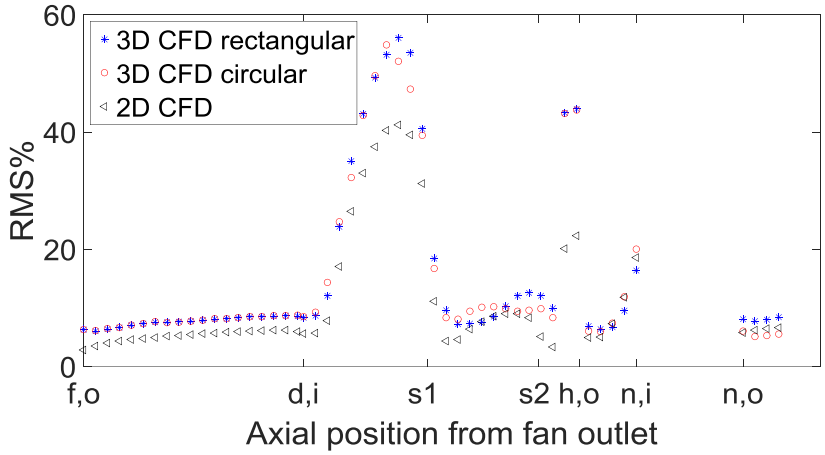

Figure 4-11: Comparison of $RMS\%$ for 2D and 3D CFD.

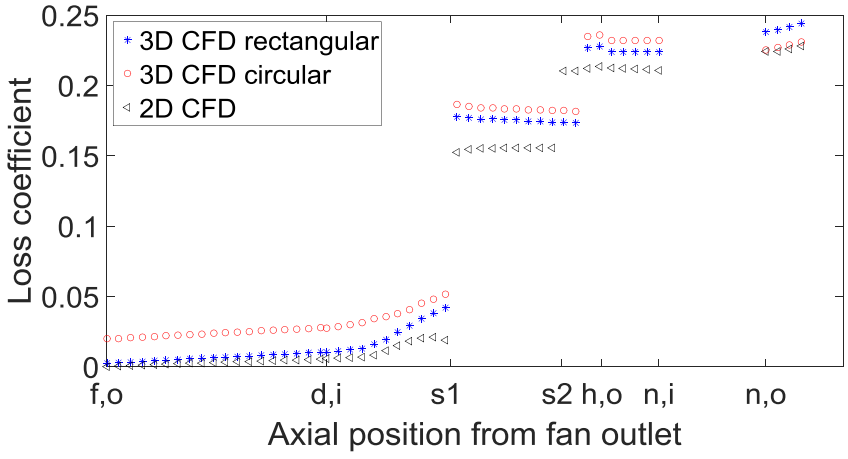

Figure 4-12: Comparison of ω for 2D and 3D CFD.

Results from the three-dimensional CFD calculations indicate that not only the flow non-uniformity and the loss coefficient are somewhat underestimated with two-dimensional CFD simulations, but the difference in the key metrics between the circular nozzle and the rectangular nozzle is not captured. This is a result of the two-dimensional CFD simulations not accounting for the change in geometry at the nozzle outlet. Yet, the two figures of merit, obtained with three-dimensional CFD calculations, are still below the threshold value set for the design, which are 10% for the $RMS\%$ and one test section inlet dynamic pressure (represented by a loss coefficient of less than 1). Therefore, since both metrics are within required range, this wind tunnel design is deemed to be successful; hence ensuring that the selected fan is sufficient for the application.

4.4 Summary of Results

With an estimated maximum total pressure loss coefficient of 0.238, and a flow non-uniformity indicated by an $RMS\%$ value of no more than 8.1%, this wind tunnel design does not just validate the use of the potential fan, but it also verifies the application of the approach that was followed. It is seen that the first principles-based approach yields the right components to meet the constraints set. Two-dimensional CFD as well as three-dimensional CFD are both essential to such a design project; two-dimensional CFD enables the sizing of the system components without prohibitive computation cost, while the three-dimensional CFD verifies the metric values for the design and captures any flow behaviour which is overlooked with two-dimensional CFD.

As seen from Fig. 4-13, using the potential fan, a margin of about 310 Pa is available to account for any additional loss by future added features such as an increased number of screens, a rise in the screen solidity ratio, or a silencer.

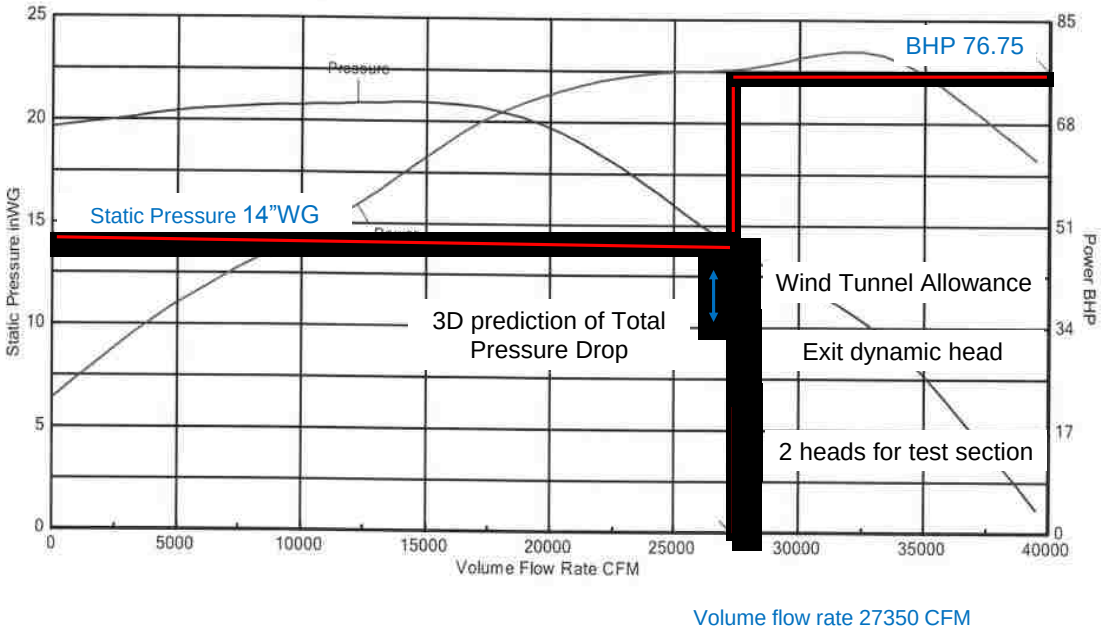

Figure 4-13: Fan providing margin for additional total pressure drop.

Chapter 5

Implementation of Wind Tunnel

In this chapter, installation, manufacturing, and commissioning-related aspects of the wind tunnel are discussed.

5.1 Additional Features of this Wind Tunnel

CAD drawings of the wind tunnel assembly, as seen in Fig. 5-1, are used for manufacturing purposes. As indicated in the figure, in addition to the wind tunnel components, gaskets are used in between each component to prevent leakage of the flow.

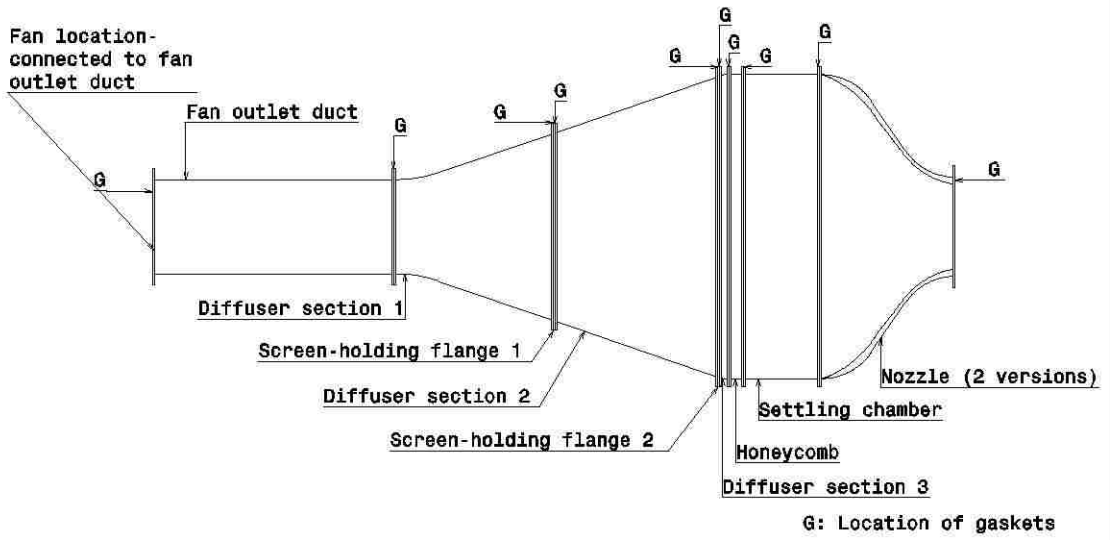

Figure 5-1: Wind tunnel assembly for manufacturing.

To enhance the performance of the wind tunnel within the facility, the following features, as illustrated in Fig. 5-2 are adopted:

- A silencer is attached at the inlet of the blower to reduce the high level of noise when the fan is operated at full speed. This also ensures fan vibration reduction. This device leads to an additional total pressure drop of 62.2 Pa, leaving about 80% of the margin for any other features.
- A variable frequency drive is used to control the AC motor/fan speed.
- Ribs, as per the expertise of the manufacturer, are introduced along the wind tunnel to reduce vibration.

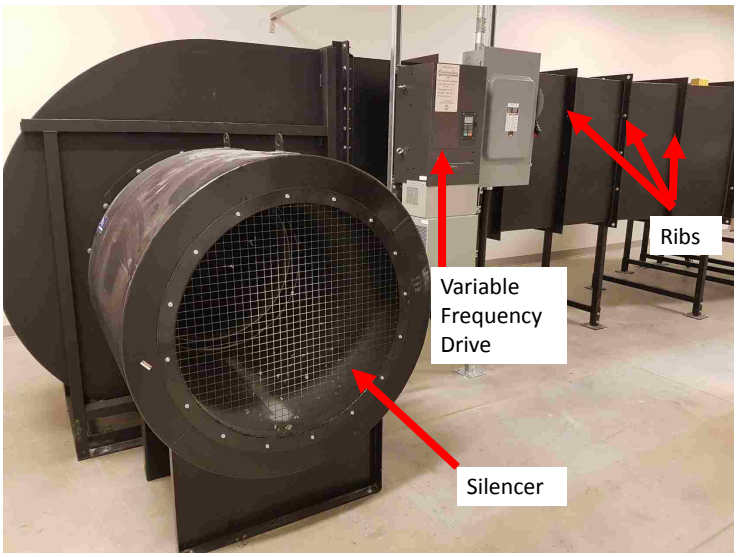

Figure 5-2: Enhancement features of the wind tunnel.

5.2 Manufacturing of the Wind Tunnel

Made out of steel, the entire duct system, up to the nozzle inlet, is manufactured by cutting the walls and welding them together. To prevent disruption in the fluid flow, angled flanges, as seen in Fig. 5-3, are used to maintain the diffusion angle.

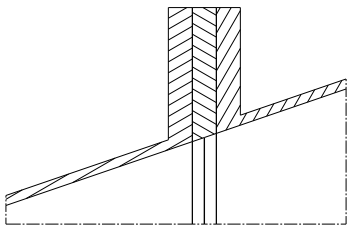

Figure 5-3: Angled flange to hold screen.

The honeycomb, made of aluminum with selected cell size given by the numerical calculations, is purchased ready-made from PLASCORE. At the outlet of the mixing chamber, clamps, as seen in Fig. 5-4, are used to allow easy and quick assembly/disassembly of the nozzles. The two nozzles, supported by frames on casters, are

manufactured differently. The illustrated features enable the easy relocation of the nozzles, once disassembled from the wind tunnel.

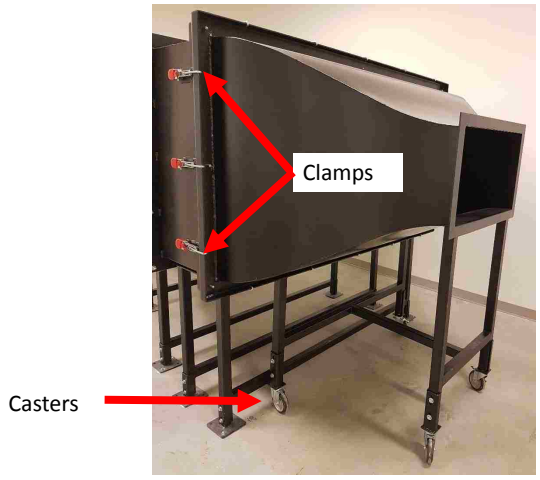

Figure 5-4: Clamps and casters for easy assembly and disassembly of nozzle.

The rectangular nozzle is created by first cutting a flattened form of the side walls which are then bent to obtain the radii of curvature; these are then welded together. The circular nozzle, the most challenging component of the wind tunnel in terms of manufacturability, is made out of fibre glass. The interior of the nozzle, which is created by cutting layers of foam stacked together, is used as a mold to wind the fibre glass around, thus creating the structure of the circular nozzle.

5.3 Commissioning of the Wind Tunnel

Based on the available literature in this area, the performance of the wind tunnel will be assessed with the use of a hot wire anemometer to determine the speed of the flow. Using this equipment, the turbulence intensity can also be measured. Using pressure transducers attached to a Pitot static tube, the velocity of the flow can be measured in a time-averaged sense. A traversing system will be used to allow the movement of the measuring devices across the cross-section of the nozzle outlet.

Chapter 6

Conclusions and Recommendations

This thesis aims at providing a general approach which can be used to model other fluid flow system. In this particular case, guidelines are developed to design a wind tunnel. A conservative approach is set to provide sufficient margin in the key metrics, $RMS\%$ and ω, to account for the presence of the test sections. This chapter summarizes the achievements detailed earlier in this thesis followed by conclusions and recommendations for future work. The wind tunnel design which has been manufactured and implemented is seen in Fig. 6-1.

Figure 6-1: Final wind tunnel design implemented.

6.1 Summary

The approach in question involves an initial analysis using the first principles of fluid mechanics to assess the limiting cases based on the loss coefficient limit, the restriction on flow non-uniformity, and the dimensional constraints. Through this analysis, the different components required for the operation of the fluid flow system are identified. Two-dimensional CFD calculations are used in a parametric study to size the different components one by one from upstream to downstream. Using the sized model of the fluid flow system, three-dimensional CFD is used to ensure that the design satisfies the constraints and requirements set.

To assess the effectiveness of this approach, it is applied to a wind tunnel design problem for the University of Windsor. This approach provides a systematic way of approaching the design of internal flow systems. A key outcome of the preliminary analysis is an estimate of tunnel losses; this enables selection of a candidate fan which can provide sufficient pressure rise to drive the flow through the wind tunnel.

Considering the required performance of the wind tunnel, an analysis of the limiting cases provides an overall system operating between the two limits. Wind tunnel comprises a fan followed by a constant area duct, which allows the development of a symmetrical velocity profile. To ensure mixing at low speed, hence reducing the fan power requirement, a diffuser is required to slow the flow. It is followed by a flow straightener, comprising a honeycomb structure and a mixing chamber, to enhance flow mixing at the diffuser outlet. To accelerate the flow to the required speed, a nozzle is introduced downstream from the straightener.

Based on 2D CFD results, due to the space requirements in this project, a wide angle diffuser, with diffusion angle of 37.8°, is chosen for this wind tunnel. Modelled as porous jumps, two screens, located at $0.475L_d$ and $0.900L_d$, act as boundary layer control devices. The computations demonstrate the requirement for a $0.163w$ long honeycomb structure comprising $0.0414w$ cell size elements, represented as thin par-

allel lines, within the wind tunnel to reduce flow non-uniformity. To further mix the region of jets and wakes in the honeycomb outflow, a $0.816w$ long mixing chamber is needed. To provide sufficient space for the test sections a $1.47w$ long nozzle with $0.653w$ radii at the inlet and outlet is adopted.

Results from 3D numerical calculations indicate that the two-dimensional CFD captured the correct flow behaviour along the wind tunnel. However, a maximum increase of 2.23% and 6.25% in flow non-uniformity and loss coefficient are noted, with the rectangular nozzle attached, when compared to the two-dimensional case. This is attributed to the lack of consideration of the second pair of walls in the wind tunnel, and added friction by the honeycomb's cell walls by the two-dimensional CFD simulations. Since the results indicate that the flow metrics of concern are within range, and the selected fan is sufficient for the application, this wind tunnel design is considered to be the final design.

6.2 Conclusions

This thesis illustrates a successful approach for the design of internal fluid flow systems. This approach yields an open loop configuration, driven by a pusher style fan, for the wind tunnel design problem established by the University of Windsor. By considering the large flow turning required and the variety in test sections, a first principles analysis enables the identification of the required components for this facility. By narrowing down the system to a particular configuration, 2D CFD is used to perform a parametric study which determines the best geometry of each component of the wind tunnel. To obtain a more accurate performance of this system, detailed 3D numerical calculation is performed. The approach is general and can be applied to a variety of internal flow systems.

To allow flow from the fan to develop into a symmetrical velocity profile, a constant

area duct is attached at the fan outlet. This is followed by a diffuser which provides a low flow speed at the inlet of the flow straightener section. The positive pressure gradient within the diffuser coupled with its aggressive nature lead to the need for screens to reduce the flow non-uniformity resulting from flow separation. Mixing of the flow at low speed, within the honeycomb, reduces the power requirement of the fan. While breaking down the large-scale flow structures in the diffuser outflow, a honeycomb creates a region of jets and wakes. To further mix this flow, a certain length of constant area duct is required before it reaches the nozzle inlet. A nozzle, due to its decreasing cross sectional area, accelerates the flow into the test section.

2D CFD simulations of different screen locations within the diffuser indicate the need for two screens, located at $0.475L_d$ and $0.900L_d$. These simulations allow the determination of the right screen locations; also, through contour plots and other visual means, they provide an understanding of the underlying reason behind the fluctuation of the figures of merit for different screen locations. Therefore, 2D CFD is essential to identify locations of critical values for the figures of merit, and to understand what flow behaviour is causing the fluctuations.

Further, contour plots of the velocity for the 2D and 3D simulations indicate that two-dimensional CFD is sufficient to capture the overall fluid flow behaviour such that the wind tunnel components can be sized without any expensive three-dimensional CFD computations. However, the latter is still required to provide a better prediction of the performance of the system.

Estimated performance, using 3D CFD computations, is found to be a maximum $RMS\%$ of 8.07% and the highest ω obtained is 0.238. Results indicate that the resulting wind tunnel design provides flow non-uniformity, within the limits imposed, to the test section inlet, and the fan can provide sufficient static pressure rise. Subsequent commissioning tests will provide an assessment of the flow quality in the wind tunnel itself.

6.3 Recommendations for Future Work

Based on the insight gained from applying this approach to the wind tunnel design, the following recommendations are made for future work:

1. While applying this approach, it is suggested that the manufacturer or contractor be involved during the two-dimensional CFD phase. Consulting with the manufacturer throughout this phase of the design would indicate if the components being simulated are easily manufactured, and if not, what the cost implications would be. Also, alternatives to these features can be proposed, simulated and assessed, thus preventing the unnecessary simulations of those features that would be impractical to manufacture. This suggestion, which will definitely increase the cost of the design phase, is beneficial in the long run as it avoids simulating unfeasible design and can significantly reduce manufacturing costs.

2. One of the few features of this wind tunnel design that requires further investigation is how the screen solidity affects the performance. While it is obvious that the losses will increase with a higher solidity, the trend for the flow non-uniformity is not clear. To determine the best solidity to achieve low $RMS\%$, various solidities should be investigated. Further, different modelling procedures for the screen could be investigated. For instance, perforated plates, with the same solidity, can be modelled in the simulations.

3. The outcomes of this study agree with the findings made by Barlow [6] indicating that a lower length to hydraulic diameter ratio of the honeycomb adversely affects the flow features. For the case where a compact honeycomb is not a requirement, honeycombs with ratio higher than the upper limit, suggested by the study, could be simulated to determine how the fluid flow is affected.

4. To achieve lower flow non-uniformity with this wind tunnel, the case of this design with a screen at the nozzle inlet should be simulated and assessed before implementing it. This is to ensure that the increased total pressure drop does not overshadow the benefits of lower flow non-uniformity.

5. The presence of filleted corners at the outlet of the rectangular nozzle should be investigated. The presence of a curved surface has the potential to reduce the flow non-uniformity created at the corner, where the two boundary layers meet. By performing this investigation, the required fillet radius can be determined to achieve the lowest flow non-uniformity.

Bibliography

[1] Dixon, S. L., and Hall, C. *Fluid mechanics and thermodynamics of turbomachinery.* Butterworth-Heinemann, 2013.

[2] Vivek, V., Sharma, A. K., and Balaji, C. A cfd based approach for thermal hydraulic design of main vessel cooling system of pool type fast reactors. *Annals of Nuclear Energy*, 57:269–279, 2013.

[3] Calautit, J. K., Chaudhry, H. N., Hughes, B. R., and Sim, L. F. A validated design methodology for a closed-loop subsonic wind tunnel. *Journal of Wind Engineering and Industrial Aerodynamics*, 125:180–194, 2014.

[4] Mehta, R. D. The aerodynamic design of blower tunnels with wide-angle diffusers. *Progress in Aerospace Sciences*, 18:59–120, 1979.

[5] Boyle, M. T. Low speed wind tunnel testing. In *Semiconductor Thermal and Temperature Measurement Symposium, 1988. SEMI-THERM IV., Fourth Annual IEEE*, pages 31–39, 1988.

[6] Barlow, J. B., Rae, W .H., and Pope, A. *Low-speed wind tunnel testing.* John Wiley & Sons, 1999.

[7] Cattafesta, L., Bahr, C., and Mathew, J. Fundamentals of wind-tunnel design. *Encyclopedia of Aerospace Engineerin*, 2010.

[8] Bradshaw, P. A low-turbulence wind tunnel driven by an aerofoil-type centrifugal blower. *Journal of the Royal Aeronautical Society*, 71:132–134, 1967.

[9] Mehta, R. D. and Bradshaw, P. Design rules for small low speed wind tunnels. *The Aeronautical Journal (1968)*, 83(827):443–453, 1979.

[10] Reneau, L. R. and Kline, S. Effects of inlet conditions on performance of two-dimensional subsonic diffusers. *J. Basic Eng*, 83(3):349–360, September 1961.

[11] Moore, C. A., and Kline, S. J. Some effects of vanes and of turbulence in two-dimensional wide-angle subsonic diffusers. Technical report, Stanford University, 1958.

[12] Cochran, D. L., and Kline, S. J. *The use of short flat vanes for producing efficient wide-angle two-dimensional subsonic diffusers.* PhD thesis, Dept. of Mechanical Engineering, Stanford University., 1957.

[13] Feil, O. G. Vane systems for very-wide-angle subsonic diffusers. *Journal of Basic Engineering*, 86:759–764, 1964.

[14] Reneau, L. R., Johnston, J. P., and Kline, S. J. Performance and design of straight two-dimensional diffusers report pd-8. Technical report, Thermosciences Division, Mechanical Engineering Department, Stanford University, 1964.

[15] Greitzer, E. M., Tan, C. S., and Graf, M. B. *Internal flow: concepts and applications.* Cambridge University Press, 2007.

[16] Cornell, W. G. Losses in flow normal to plane screens. *Trans. ASME*, 80:791–799, 1958.

[17] Noui-Mehidi, M. N., Wu, J., Šutalo, I. D., and Grainger, C. Velocity distribution downstream of an asymmetric wide-angle diffuser. *Experimental thermal and fluid science*, 29(6):649–657, 2005.

[18] Sahin, B., and Ward-Smith, A. J. The use of perforated plates to control the flow emerging from a wide-angle diffuser, with application to electrostatic precipitator design. *International journal of heat and fluid flow*, 8(2):124–131, 1987.

[19] Hales, T. C. The honeycomb conjecture. *Discrete & Computational Geometry*, 25(1):1–22, 2001.

[20] Morel, T. Comprehensive design of axisymmetric wind tunnel contractions. *J. Fluids Eng*, 97(2):225–233, 1975.

[21] Bardina, J., Huang, P., Coakley, T. Turbulence modeling validation. In *28th Fluid dynamics conference*, page 2121, 1997.

[22] Menter, F. R. Two-equation eddy-viscosity turbulence models for engineering applications. *AIAA journal*, 32(8):1598–1605, 1994.

[23] Wilcox, D. C. *Turbulence modeling for CFD*, volume 2. DCW industries La Canada, CA, 1998.

[24] Launder, B. E. and Sharma, B. I. Application of the energy-dissipation model of turbulence to the calculation of flow near a spinning disc. *Letters in heat and mass transfer*, 1(2):131–137, 1974.

[25] Spalart, P. and Allmaras, S. A one-equation turbulence model for aerodynamic flows. In *30th aerospace sciences meeting and exhibit*, page 439, 1992.

[26] Moonen, P., Blocken, B., Roels, S., and Carmeliet, J. Numerical modeling of the flow conditions in a closed-circuit low-speed wind tunnel. *Journal of Wind Engineering and Industrial Aerodynamics*, 94(10):699–723, 2006.

[27] Harvey, S. A. *Low-speed wind tunnel flow quality determination.* PhD thesis, Monterey, California. Naval Postgraduate School, 2011.

[28] NorthernBlower. Air performance curve. Technical report, January 2017.

[29] Sugarman, S. C. *HVAC Fundamentals.* Fairmont Press, Inc., 3 edition, 2016.

[30] Air Movement and Control Association. *AMCA Fan Application, "AMCA Publication 201"*, 1973.

[31] ANSYS Inc. *ANSYS Fluent User's Guide, Version 17.0.* Canonsburg, PA, November 2013.

Vita Auctoris

Name	Kharuna Ramrukheea
Place of Birth	Curepipe, Mauritius
Year of Birth	1990
Education	University of Windsor, Windsor ON 2009-2014 B.A.Sc.
	University of Windsor, Windsor ON 2015-2017 M.A.Sc.